Helmholtz-Zentrum Geesthacht
Zentrum für Material- und Küstenforschung

Final Draft
of the original manuscript:

Kowalczuk, P.; Tilstone, G.H.; Zablocka, M.; Roettgers, R.; Thomas, R.:
Composition of dissolved organic matter along an Atlantic Meridional Transect from fluorescence spectroscopy and Parallel Factor Analysis
In: Marine Chemistry (2013) Elsevier

DOI: 10.1016/j.marchem.2013.10.004

Composition of Dissolved Organic Matter along an Atlantic Meridional Transect from fluorescence spectroscopy and Parallel Factor Analysis.

Piotr Kowalczuk[1], Gavin H. Tilstone[2], Monika Zabłocka[1], Rüdiger Röttgers[3], and Rob Thomas[4]

[1] Institute of Oceanology, Polish Academy of Sciences, ul. Powstańców Warszawy 55, PL-81-712, Sopot, Poland

[2] Plymouth Marine Laboratory, Prospect Place, The Hoe, Plymouth PL1 3DH, United Kingdom

[3] Institute for Coastal Research, Helmholtz-Zentrum Geesthacht, Centre for Materials and Coastal Research, Max-Planck-Str. 1, D-21502 Geesthacht, Germany

[4] British Oceanographic Data Centre, Joseph Proudman Building, 6 Brownlow Street, Liverpool, L3 5DA, United Kingdom

Manuscript revision 2, November 21, 2013

Submitted to editors of Marine Chemistry

Abstract

Absorption spectra and induced fluorescence excitation emission matrices of colored dissolved organic matter were measured in water samples collected along the Atlantic Meridional Transect in different bio-geographic provinces of the Atlantic Ocean from October-November 2010. The highest values of CDOM absorption coefficient at 305 nm ($a_{CDOM}(305)$), were recorded at the continental margins of the English Channel and Patagonian Shelf. The lowest values of $a_{CDOM}(305)$ were observed in the mixed layer of both North and South Atlantic subtropical oligotrophic gyres. The DOM composition was assessed using fluorescence spectroscopy, Excitation Emission Matrix spectra (EEMs) and the Parallel Factor Analysis (PARAFAC) model in addition to spectral indices calculated from CDOM absorption spectrum and EEMs spectra. Six different components were identified in the EEMs by PARAFAC: Two components were similar to the humic-like fraction of DOM, associated with basin scale microbial mineralization processes. These components represent allochthonous DOM in the biogeographic provinces studied. One component of marine humic-like material of autochthonous origin, associated with DOM production from marine phytoplankton. Three components were associated with protein-like DOM. Two protein-like components had the spectral characteristics of pure tryptophan and tyrosine. There was a significant difference in DOM composition both between bio-geographical provinces and above and below the mixed layer. In the mixed layer in all provinces, except the waters of the Western European Shelf, the DOM was dominated by protein–like components. At the Western European Shelf, it was dominated by humic-like components. Fluorescence intensities of humic-like components were high at the Patagonian Shelf, but were up to 40% lower compared to Northern Hemisphere shelf waters. Humic-like components made a significant contribution to the DOM composition of the upper mesopelagic layer in all provinces, with the highest values at the Equatorial Upwelling zone. There was a significant inverse relationship between humic-like components and salinity and temperature and a positive relationship with Apparent Oxygen Utilization. The humification index (HIX) was linearly correlated with the intensity of the humic-like DOM components. These trends suggest that the humic-like components are in dynamic equilibrium between likely microbial production in the deep ocean and photochemical degradation in the mixed layer.

1. Introduction

Dissolved organic matter (DOM), is by far the largest pool of organic matter in the sea. About 97% of all organic carbon in the marine environment is incorporated into DOM with an estimated 665 Pg C as dissolved organic carbon (DOC) (Hansell, 2013). The mass of DOC in the sea is comparable with the mass of carbon in the Earth's atmosphere, as CO_2, and the amount of carbon stored in terrestrial ecosystems (Hedges, 2002). The dominant source of organic matter in the world's ocean is autochthonous production, which accounts for more than 95% of the total organic matter. DOM is regarded as a large inert reservoir of carbon in the ocean, which below the mixed layer is isolated from the present carbon cycle. Results of recent studies have changed this paradigm and revealed that DOM is an active and dynamic component in carbon biogeochemical cycles and plays an important role in marine ecosystems (e.g. Jiao et al., 2011). DOM consists of a complex mixture of organic compounds resulting from the breakdown of bacteria, algae and/or higher plants and their continuous transformation through photochemical and microbial processes. Due to their complexity, most DOM in the ocean (>85%) have not been characterized (Benner, 2002). The compounds that have been identified are mainly low or medium molecular weight organic molecules: hydrocarbons, carbohydrates, fatty acids, and amino acids (Benner 2002). There is insufficient knowledge about the remaining fractions of organic matter, which consist mainly of medium and high molecular weight compounds (e.g. proteins, lipids and their polymers and complexes with phenols and metals). There are two major fractions of humic substances present in aquatic environments: humic and fulvic acids, that differ from each other by molecular weight, chemical composition, chemical properties, aromaticity and optical properties (Harvey et al., 1983; Carder et al., 1989).

The optically active fraction of DOM, especially humic substances, called chromophoric dissolved organic matter (CDOM), is one of the major determinants of the optical properties of natural waters, directly affecting both availability and spectral quality of light in the water column (Jerlov, 1976; Blough and Del Vecchio, 2002). In the pelagic ocean absolute concentrations of CDOM, expressed as the magnitude of the CDOM absorption coefficient $a_{CDOM}(\lambda)$, are extremely low (Nelson and Siegel, 2002). In relative terms, however, the contribution of CDOM to the total absorption of oceanic waters is very high and may reach, in the clearest oceanic waters, more than 90% in the ultraviolet range of electromagnetic spectrum (Morel et al., 2007; Bricaud et al., 2010; Tedetti et al., 2010). CDOM also causes significant attenuation of ultraviolet light in the ocean (Smyth, 2011).

Through this process, CDOM is transformed photochemically into inorganic carbon, low-molecular-weight organic compounds, trace gases, phosphorus- and nitrogen-rich compounds (e.g. Vähätalo and Zepp, 2005; Stedmon et al., 2007). CDOM has the ability to become complexed with trace metals, which can be released through the remineralization of DOM. It is therefore fundamental for better understanding of biogeochemical cycles in the oceans, to differentiate and quantify sources of CDOM and analyze the underlying factors that lead to its variability.

A proportion of the CDOM has an inherent ability to fluoresce. This characteristic is well known (Duursma, 1974) and has been used to estimate CDOM in a range of natural waters (Hoge et al., 1993; Vodacek et al., 1997; Ferrari and Dowell, 1998; Ferrari, 2000). One application of the fluorescence spectroscopy technique is to measure the Excitation Emission Matrix (EEM) (Coble, 1996) through detecting the emission spectra at a series of successively increasing excitation wavelengths. Multivariate statistics can then be used to interpret the resulting EEM spectra (Stedmon et al., 2003), which enables discrimination of different classes of fluorophores based on their excitation/emission maxima. This approach is advantageous when used to interpret the multidimensional nature of EEMs data sets, to study variability of DOM in coastal areas (Stedmon and Markager, 2005a). The technique has undoubtedly, improved our understanding of production and degradation processes of DOM fluorescence in the marine environment (Stedmon and Markager, 2005b), and has become a useful tool for tracing anthropogenic pollutants or terrestrial inputs to the oceanic DOM pool (Murphy et al., 2006; Murphy et al., 2008).

The distribution of CDOM optical properties along the Atlantic Meridional Transect and its role in photochemical production of carbon monoxide has been studied during previous AMT cruises (Kitidis el al., 2006; Stubbins et al., 2006). The detailed compositional structure of the DOM remains to be quantified. The main objectives of this study were to: i) use the fluorescence spectroscopy technique and PARAFAC, optical properties of CDOM absorption and their spectral indices to assess the composition of the DOM and their spatial variability in both the epipelagic and top of the mesopelagic layers in a range of Atlantic Ocean provinces, ii) from these, to identify regions of enhanced degradation and localized production of fluorescent DOM fractions, iii) to discriminate allochtonous fractions of DOM produced outside of the Atlantic biogeographic provinces by different bacterial, viral or phytoplankton communities over different spatial and temporal scales, iv) and to discriminate the autochthonous fraction of DOM produced within the biogeographic provinces by bacterial, viral or phytoplankton communities over much shorter time scale.

2. Materials and Methods

2.1 *The study area*.

The Atlantic Meridional Transect (AMT) program is a long time data series that started in 1995. The research is conducted on Natural Environment Research Council-UK (NERC) ships between the UK and the Southern Ocean and has currently been under taken on 23 cruises. AMT20 was aboard the RRS "James Cook" between 13 October and 21 November 2010 from Southampton, UK, to Punta Arenas, Chile. Sampling was conducted in six biogeochemical provinces: North Atlantic Drift (NADR), North Atlantic Subtropical Gyre (NAST), North Atlantic Tropical Gyre (NATR), Western Tropical Atlantic (WTRA), South Atlantic Subtropical Gyre (SATL), South Subtropical Convergence (SSTC) (Longhurst, 1995), to characterize the variability in CDOM over a range of oligotrophic, eutrophic and mesotrophic environments in the Atlantic Ocean. The stations sampled during AMT20 were principally in the North and South Atlantic Gyres, but the productive waters of the Celtic Sea, Patagonia shelf and the Equatorial upwelling zone were also sampled. Data collected in the tropical zone in the NATR and WTRA were pooled together to achieve a larger sample size for statistical analyses (see Table 1). The data from the subtropical Southern Atlantic zone were also pooled for the same reason, except for the three last sampling stations which were located close to the Patagonian Shelf. These latter stations bordered the subtropical front where there was an austral spring Coccolithophore bloom. The following regions were therefore defined to analyze salient trends in DOM: European Continental Shelf Waters (WES), North Atlantic Subtropical Gyre (NAST-E), Equatorial Upwelling (EQU), South Atlantic Subtropical Gyre (SATL), and Patagonian Shelf (PAS).

2.2. *Samples collection and processing and spectroscopic measurements*

Water samples were collected from mid-morning (1100–1200 h local time) deployments of a Sea-Bird water sampling rosette equipped with a Sea-Bird SBE 911 *plus* CTD unit, fitted with a Chlorophyll-*a* fluorometer (Chelsea Technologies Group Aquatracka MKIII) and a dissolved oxygen concentration sensor (Sea-Bird SBE43). CTD conductivity data were converted to absolute salinity [g kg^{-1}] using the algorithm developed by McDougall et al., (2012). The following depths were sampled at all stations: 300, 200, 100 and 0 m. In addition, if not co-incident with these depths, samples from the Deep Chlorophyll Maximum (DCM), bottom of the mixed layer and middle of the mixed layer were also taken. A total number of 214 water samples were collected from 35 stations (Figure 1). The samples were

measured immediately onboard the ship for determination of CDOM absorption and fluorescence EEM, and processed using a two-step filtration: firstly through acid-washed Whatman glass fiber filters (GF/F, nominal pore size 0.7 μm), secondly through acid-washed Sartorius 0.2 μm pore size cellulose membrane filters to remove finer particles. The samples were allowed to warm to room temperature prior to spectroscopic and spectrofluorometric scans.

The CDOM absorption coefficient was measured using a liquid wave guide capillary cell system (LWCC-2100, WPI Inc, USA) with a nominal optical pathlength of 1.094 m, according to the methods described by D'Sa et al., (1999) and Miller et al., (2002). Light is axially introduced into the waveguide via an optical fiber and is transmitted and constrained within the capillary cell by total internal reflection. The light source was a UV/VIS lamp (DH-2000-S, Ocean Optics, USA) equipped with an electronic shutter. At the opposite end of the waveguide, a detection fiber conducts the light that is not absorbed by the aqueous medium to a fiber-optics-based spectrometer that uses a diffraction grating to disperse the transmitted light into a CCD detector array (USB-4000, Ocean Optics, USA). There is an inlet or outlet connection at each end of the waveguide for injecting filtered seawater samples or any other aqueous solution. The injected volume of sample was usually less than 4-5 ml. Before and after injection of the sample volume the capillary waveguide cells were flushed and filled with purified water for blanking. Measurements of absorbance (250 – 800 nm) were performed using the SpectraSuite software (Ocean Optics, USA). Each sample has been measured with the LWCC system in triplicate to ensure repeatability, after the dark current of the detector was set with the help of the shutter and the reference blank was set with MilliQ water. Raw recorded absorbance $A(\lambda)$ spectra were processed and the true CDOM absorption coefficients $a_{CDOM}(\lambda)$ in $[m^{-1}]$ were calculated by:

$$a_{CDOM}(\lambda) = 2.303 \cdot A(\lambda)/L, \quad (1)$$

where L is the optical path length and the factor 2.303 is the natural logarithm of 10. The spectral data were then corrected for the influence of salinity on pure water absorption and refractive index. A salinity correction spectrum was recorded by measuring a 100g/l NaCl solution (assumed to be ~100 PSU) made from combusted 99.99 % pure NaCl salt. The corrected spectra of the true CDOM absorption coefficient were used to calculate the CDOM absorption spectrum spectral slope coefficient with use of a non-linear regression technique at spectral range 250 - 600 nm, $S_{250\text{-}600}$, which provides accurate coefficients for modeling

(Stedmon et al., 2000). This spectral slope coefficient can be used to model the entire CDOM absorption spectrum, (Stedmon and Markager, 2003; Kowalczuk et al., 2006), and is directly comparable with methods used for remote sensing (Swan et al., 2013). The recent review by Nelson and Siegel (2013) highlighted the importance of the accurate calculation of the CDOM spectral slope coefficient in the global ocean to improve ocean color remote sensing products, which is why we used this spectral range to calculate the slope coefficient. The linear regression model was used to calculate spectral slope coefficient at two different spectral ranges: 275 - 295 nm, $S_{275\text{-}295}$, and 350 – 400 nm, $S_{350\text{-}400}$. The spectral slope coefficients $S_{275\text{-}295}$ and $S_{350\text{-}400}$ were then used to calculate the slope ratio, S_R, following Helms et al., (2008).

Samples for fluorescence analysis were treated in the same way as the absorption measurements. DOM fluorescence measurements were made on a Varian Cary Eclipse scanning spectrofluorometer in a 1 cm pathlength quartz cuvette using a 4 ml sample volume. A series of emission scans (280–600 nm at 2 nm resolution) were taken over an excitation wavelength range from 240 to 500 nm at 5 nm increments. The instrument was configured to collect the signal using maximum lamp energy and 5 nm band pass on both the excitation and emission monochromators. The excitation and emission matrix spectra were processed according to procedures described by Stedmon and Bro, (2008) and Murphy et al., (2010). Samples were spectrally corrected with a set of instrument dependent correction coefficients and calibrated against the Raman scatter emission peak of a MilliQ water sample, run on the same day, excited at the wavelength of 350 nm and integrated in the spectral range 374 – 424 nm. The Raman normalization and correction procedures resulted in spectra that are in Raman units (R.U., nm^{-1}) and are directly comparable to corrected spectra measured on other instruments. Samples were not corrected for inner filter effects, as the CDOM absorption coefficients for all samples in the whole excitation and emission spectral ranges were 10 times smaller than a threshold value above which this correction is necessary (Stedmon and Bro 2008). Following this, a Raman normalized EEM of MilliQ water was subtracted from the data to remove the Raman signal.

2.3. *PARAFAC model*.

The corrected and calibrated EEM spectra were statistically analyzed using the methods described by Stedmon et al., (2003), and the PARAFC model was run using the ‘‘N-way toolbox for MATLAB ver. 2.0’’(Andersson and Bro, 2002). With this technique, signals from a complex mixture of compounds (in this case, fluorescent DOM) can be

separated, with no assumptions on their spectral shape. The only assumption in the PARAFAC algorithm is that the components differ from each other spectrally. The PARAFAC model was run with a non-negativity constraint; the final dimensions of the data array were: 209 samples × 53 excitations × 151 emissions. The combined data set was split into two halves randomly called "calibration" (CAL) and "validation" (VAL) to perform a split-half validation procedure. PARAFAC was run on each CAL and VAL data group. The six component model was successfully validated in three independent data sets to ensure high accuracy of the modeled CDOM components.

The intensity of the *nth* component in a given sample, I_n, and the total fluorescence intensity, I_{tot}, were calculated using the equations given in Kowalczuk et al., (2009). The intensities of modeled EEM spectra and individual components were used to calculate spectral indices as indicators of the origin of the DOM, precursory material, degree of aromaticity and humification. The fluorescence index (FI) was calculated according to McKnight et al., (2001) as the ratio of the emission intensity at 450 nm to that at 500 nm, obtained with an excitation at 370 nm. The humification index, HIX, was calculated according to Zsolnay et al., (1999) as the ratio of the emission spectrum (excited at 255 nm) integral over the spectral range 434 – 480 nm, to the integral of emission spectrum over the spectral range 330 – 346 nm (excited at the same wavelengths). We also calculated the ratio of the sum of intensities of the protein–like components to the sum of intensities of the humic-like components as follows:

$$I_{Protein} / I_{Humic} = \frac{I_{C3} + I_{C4} + I_{C6}}{I_{C1} + I_{C2}}, \qquad (2)$$

where I_{Cn} is the intensity of respective component from C1 to C6 identified by the PARAFAC model. The spectral characteristics and origins of these are explained in the Results section and given in Table 2. The component C5 was not included in the denominator of Equation 2. This component represents low molecular weight autochthonous marine humic-like material (Coble, 1996) produced within the biogeographic provinces during localized-scale mineralization processes. Although the spectral characterization of C5 is significantly different from protein-like DOM, the meridional distribution of C5 is close to protein-like fraction of DOM that is also autochthonous (data not shown).

2.4. *Statistical analysis*.

One-way analysis of variance (ANOVA) was used to test for significant differences between provinces and below or in the mixed layer. Kolomogrov–Smirnov with Lilliefors tests were used to check whether the distribution of each parameter was normal which was log-transformed for SR and square root transformed for the other variables, until no significant difference was found between the expected and the observed distributions. The ANOVA results are given as $F_{1, 204} = x$, $P = y$ where F is the mean square to mean square error ratio, the subscript numbers denote the degrees of freedom and P is the ANOVA critical significance value.

3. Results

3.1 *Hydrography*

The distributions of temperature, salinity and density over the Atlantic Ocean during previous AMT cruises has been described by Aiken et al. (2000) and Robinson et al. (2006). The hydrography during AMT20 (Figure 2), did not deviate from the typical climatology of the salinity and temperature distribution during October-November in the North and South Atlantic. The Atlantic biogeographic provinces were clearly delineated by hydrographic fronts: Sampling started in the North Atlantic Drift (NADR) province at the eastern edge of the European Continental Shelf Waters and Celtic Sea (Figures 1 and 2). The subtropical front, that separated water masses with a surface temperature <16°C and salinity of 36 g kg^{-1}, from warmer subtropical waters, with salinity >37 g kg^{-1}, marks the boundary between NADR and the North Atlantic Subtropical Gyre (East) (NAST-E) province. Further south, the decrease in salinity to <36 g kg^{-1} and increase in sea surface temperature >28°C, indicated the boundary between NAST-E and two tropical provinces: the North Atlantic Tropical Gyre waters (NATL) and the Western Tropical Atlantic (WTRA). The salinity below <35 g kg^{-1}, indicated the trajectory of the North Equatorial Current. In the southern hemisphere, a decrease in sea surface temperature <25°C and an increase in salinity >37 g kg^{-1} in the surface water, separated the tropical provinces from the South Atlantic Gyre (SATL) province. The sea surface temperature between 15-16°C and salinity 36 g kg^{-1} characterized the South Subtropical Convergence (SSTC) province. The last 3 stations sampled during AMT20 passed through the southern sub-polar front in waters characterized by the sea surface temperature of ~11°C and salinity <35 g kg^{-1}.

The location of the thermocline illustrated that the mixed layer was relatively shallow in the NADR (~50 m) and was around 70 m in the centre of the NATL. The mixed layer

shoaled in the northern hemisphere tropical waters to 40 m south of Equator, due to the influence of Equatorial upwelling. The thermocline again deepened in the SATL reaching ca. 70 m. The water column in the SSTC and south of the sub-polar front on the Patagonian Shelf was vertically mixed. The extent of the mixed layer controlled the distribution of the deep Chlorophyll-*a* maximum (DCM) in temperate waters in the North and South Atlantic (Figure 2). The DCM in subtropical and tropical waters was found below MLD and reached 120 m in the NAST-E and 180 m in the SATL. The Apparent Oxygen Utilization (AOU) was low in the mixed layer in both northern and southern hemispheres. AOU minima were recorded in the NAST(E), NAST(W) and SSTC which were associated with an increase in Chlorophyll-*a* concentrations. Maximum AOU values were observed at 10°S at the southern edge of Equatorial Upwelling at 200 m.

3.2 *Distribution of CDOM optical properties in different water masses along AMT20 transect*

The CDOM, absorption coefficient $a_{CDOM}(\lambda)$, can be regarded as an optical proxy for DOM concentration that represents the combination of remnants of biological productivity in the marine environment and input of terrestrial organic material to the ocean (Siegel et al., 2002). The spectral slope of the absorption spectrum can be used as a proxy of DOM composition (Carder et al., 1989). The slope, however is the result of CDOM formation, through the mixing of water bodies that have different CDOM optical properties (two or multiple end members; e.g. Stedmon at al., 2010), paralleled autochthonous production (Astoreca et al., 2009) and decomposition of CDOM by UV radiation and microbial uptake (Twardowski and Donaghay, 2002; Sulzberger and Durisch-Kaiser, 2009). The spectral slope ratio, S_R, is linearly correlated with the molecular weight measured by size exclusion chromatography (Helms et al., 2008) and flow field fractionation (Guéguen and Cuss, 2011). Low values of S_R indicate high MW DOM of terrestrial origin or DOM, presumably transformed in dark microbial transformation. High values of S_R indicate low MW DOM. The humification index, HIX, is the fluorescence spectroscopy index that describes the diagenetic state of the DOM. High HIX values are characterized by high molecular weight, aromatic humic acids (Zsolnay et al., 1999).

The variability in CDOM absorption coefficient at 305 nm ($a_{CDOM}(305)$), the absorption spectrum slope coefficient $S_{250\text{-}600}$, the Helms spectral slope ratio, S_R, and the humification index, HIX, along the AMT20 track are given in Figure 3. The Table 1 gives mean ± standard deviation of CDOM optical properties and spectral indices for five

biogeographic Atlantic Ocean provinces. The $a_{CDOM}(305)$ in the mixed layer were higher in temperate and subpolar regions of the WES and PAS (0.39±0.12 m^{-1}, and 0.28±0.055 m^{-1}, respectively). There was a significant difference in $a_{CDOM}(305)$ between provinces (Table 3) with highest values in WES and lowest values in the SATL. In addition in the SATL, there was no significant difference in the vertical variability in $a_{CDOM}(305)$ between the MLD and below the MLD. The average values of the $a_{CDOM}(305)$ observed below the mixed layer were however, 44 % lower in the European Continental Shelf Waters (0.27±0.087 m^{-1}) compared to the mixed layer. On the Patagonian Shelf, the difference between average $a_{CDOM}(305)$ in the mixed layer was 27 % lower than below the mixed layer. Extremely low $a_{CDOM}(305)$ was observed in the mixed layer of both the NATL and SATL from the surface to 60 m. There was a slight increase in $a_{CDOM}(305)$ close to the equator corresponding with the equatorial upwelling between 15° N and 3° S. There were also notable increases in $a_{CDOM}(305)$ from the bottom of the mixed layer in the northern hemisphere from 45° to 25° N between 80 – 100 m, and in the southern edge of the Equatorial Upwelling Zone from 7 N° and 7° S, which corresponded to the location of the Chlorophyll-*a* maxima (Figure 2).

The distribution of the spectral slope coefficient $S_{250\text{-}600}$, showed the reverse trend. Low values of $S_{250\text{-}600}$ were observed on both, northern and southern ends of the transect, and below the mixed layer. The highest $S_{250\text{-}600}$ values of 0.038 nm^{-1} and 0.039 nm^{-1} were observed at the center of northern and southern Atlantic Subtropical Gyres. The lowest values of $S_{250\text{-}600}$ (0.021 – 0.022 nm^{-1}) were in the Equatorial Upwelling Zone below 200 m, in low temperature, salinity and oxygen. $S_{250\text{-}600}$ was significantly higher in the NAST and SATL and in the MLD (Table 3). S_R had a similar distribution. The lowest S_R values were observed at northern and southern ends of the transect ($S_R \sim 2$), on the WES and PAS, probably due to the influence of higher terrestrial DOM being transported across the shelf in both regions. Low S_R values were also observed in the uppermost mesopelagic layer at the Equator ($S_R \sim 2.5$), probably due to the upwelling of Eastern North Atlantic Central Water (ENACW). The highest values of S_R were observed in the NATL ($S_R > 4$). There was a significant difference in HIX between the mixed layer and below it and between biogeographic provinces (Figure 3). Elevated HIX values occurred in the mixed layer of the WES and PAS. On average, HIX values in the southern hemisphere were smaller (1.37±0.38) than in the northern hemisphere (1.80±0.15). The lowest values of the HIX in the mixed layer were observed in the oligotrophic gyres in the northern and southern hemispheres (0.88±0.39 and 0.66±0.31,

352 respectively). There was a 4 fold increase in HIX below the MLD in the SATL. Vertical
353 changes in HIX were smallest in the PAS. The horizontal and vertical distribution of the
354 fluorescence index (FI), were the same as the HIX, but the overall variability of this index
355 was smaller, ranging from 1.00 to 1.29. There was a significant difference in HIX both
356 vertically in the water column and between provinces.

357 3.3 *PARAFAC model output.*

358 Contour plots of individual PARAFAC components are given in Figure 4. Table 2
359 provides excitation and emission characteristics of the CDOM components with comparative
360 references for other components identified globally from oceanic and estuarine environments.
361 The PARAFAC model identified three humic-like substances: presumed substances of
362 terrestrial origin that occurred at the continental margins, substances produced in pelagic
363 ocean from microbial (prokaryotic) remineralization of DOM or produced directly by
364 phytoplankton (eukaryotic). Two major components were characterized: component 1 (C1),
365 and component 2 (C2) which are commonly found in a range of estuarine and oceanic
366 environments, and one secondary humic-like component — component 5 (C5). C1 explained
367 the highest proportion of variability in the composition of the EEMs library; with a primary
368 excitation band centered at 240 nm and the secondary excitation peak at 320 nm. The single
369 emission band of C1 has a maximum at 396 nm. This component represents humic material,
370 presumably of terrestrial origin or in situ bacterial transformation of DOM, characterized by
371 lower molecular weight and less aromatic compared to humic C2. The primary excitation
372 band of component C2 has a peak at 240 nm and the secondary excitation peak at 370 nm.
373 This component represents fluorophores that have the broadest excitation band as well as the
374 longest emission wavelength (max 480 nm) associated with a broad emission band. Such
375 excitation and emission characteristics are associated with terrestrial organic matter that is
376 composed of high molecular weight and aromatic organic compounds (McKnight et al., 2001;
377 Stedmon et al., 2003). The most recent experimental studies based on production of
378 fluorescence fraction of DOM, have provided evidence that C2 (peak C, Coble, 1996) could
379 be a product of microbial (prokaryotic) remineralization of marine phytoplankton exudates
380 (Romera-Castillo et al., 2011). Component 5 (C5) (ex. 300 nm/em. 408 nm) represents marine
381 humic substances and dissolved organic matter that has been altered by microbial recycling
382 (Stedmon and Markager, 2005b). Recent results from mesocosm experiments have shown that
383 axenic cultures of common phytoplankton groups can release DOM exudates that have optical
384 characteristics similar to C5 (Romera-Castillo et al., 2010; 2011). There were three

components, C3, C4, and C6 that have excitation/emission characteristics with narrow excitation bands, and emission maxima below 400 nm, that are similar to fluorescent protein-like compounds. These are presumably a combination of fluorophores containing the fluorescent amino acids; phenylalanine, tryptophan and tyrosine and / or free amino acids or amino acids bound in protein molecular structures. These components contain fractions of autochthonous DOM. Component 3 (C3) has narrow excitation band, is similar to tyrosine component 4 (C4), but it also has a broad emission band that is similar to a tryptophan –like component C6 (C6). This may reflect protein-like fluorescence components that exhibit spectral properties of tyrosine and tryptophan bound into larger structures of organic molecules rather than pure compounds diluted in seawater. The excitation/emission maxima of the C3 component are very close to unclassified component C6 found by Jørgensen et al. (2011) in the open ocean, world-wide. Tryptophan and tyrosine bound together in the same protein can also undergo energy transfer which can have has complex effects on the fluorescence (Moens et al., 2004).

3.4 *Distribution of DOM components along the AMT20 transect*

Differences in the composition of DOM from the PARAFAC model in the different biogeographic provinces and within and below the mixed layer are quantified in Table 3. To summarize these, Figure 5 presents the average composition of DOM fluorescence EEMs components in and below the mixed layer in five sampled biogeographic provinces. There was a consistent pattern of DOM composition in the surface layer and DOM components in the NAST-E, EQU and SATL were ranked with the same order of abundance: C4>C3>C6>C5>C1>C2. This compositional pattern was also found in all samples collected above the pycnocline. The protein–like component C3 and marine humic-like component C5 were significantly different between provinces and in and below the mixed layer, with higher values for C3 in the MLD and higher values for C5 below the MLD. C3 was higher in the WES, whereas C5 was highest in the EQU (Table 3). There was a significant difference between C4 and C6 between provinces, with significantly higher values in the NAST and EQU, but there was no difference in and below the mixed layer (Table 3).

In addition, the intensity of humic like components C1 and C2 were significantly higher in the WES and EQU and below the mixed layer (Table 3), and on average C3>C1>C4>C5>C2>C6. The high intensity of C1 indicates the impact of terrestrial organic matter on this province. The other terrestrial DOM component C2 was ranked fifth, but its intensity was similar to C4 and C5. The composition of the humic-like components C1 and

C2 were on average 30 % and 20% lower in the PAS, which was different from that in the shelf waters of the WES. The intensity of DOM components in the surface waters of the PAS were C4>C3>C5>C1>C6>C2, which suggest a relatively low contribution of humic-like material and a relatively higher contribution of marine humic-like C5, possibly due to the release of freshly produced DOM by phytoplankton from a Coccolithophorid bloom that occurred in the area (data not shown).

C1, C2, C4 and C5 were significantly higher below the mixed layer than above it (Table 3), whereas there was no difference in C3 and C6 above and below the MLD. The two fold increase in C5 below the mixed layer corresponds to an increase in marine humic-like substance at depth in all provinces. There were also notable differences in composition between biogeographic provinces. In the WES mesopelagic waters, for the DOM components C1>C3>C2>C5>C6>C4 and the intensity of the tyrosine component C4 was the lowest. By contrast, in the NAST-E the component ranking: C1>C4>C5>C3>C2>C6 indicated an increase in the tyrosine like component C4. The composition of DOM in the EQU and in the SATL were similar with C1>C4>C5>C2>C6>C3 in the EQU and C4>C1>C5>C6>C2>C3 in the SATL. The intensity of C4 was slightly higher than intensity of the C1 in the SATL compared to EQU. In addition, C6 was higher than C2 in the other provinces. The composition of DOM above and below the MLD in the PAS was similar, with a slight change in the ranking of C3 and C5 between them. In the PAS, the intensity of C3 was higher in the mixed layer than below it and whereas that of C5 was lower in the mixed than below it.

The meridional section of total DOM fluorescence intensity I_{Tot}, the intensities of the humic-like and protein-like fractions of the DOM fluorescence and the ratio: $I_{Protein}/I_{Humic}$ is given in Figure 6. There were significant differences in both the vertical and zonal distribution in I_{Tot}, humic-like, protein-like and $I_{Protein}/I_{Humic}$ (Table 3), especially at 10° N in the subsurface waters between 100 – 200 m of the EQU, and in the SATL to the PAS at shallower depths, (Figure 6). This belt of high fluorescent water corresponds with the meridional section of the $I_{Protein}$. The uncharacterized protein-like C3 was abundant in the surface layer, euphotic layer, between 0 and 200 m, and was evenly distributed over depth, and its intensity was negligible below 200 m. The intensity of C3 was greater in the southern hemisphere than in the northern hemisphere, and was significantly lower in the NAST-E (Table 4). The tyrosine-like component C4 contributed most to the DOM fluorescence and was highest at 10° N at a depth of between 100 and 200 m. The intensity of the tryptophan-like C6 was highest in the NAST-E in the mixed layer and became sub-ducted southward with

a maximum at 100 m in the SATL parallel to 25° S. Its intensity in the northern hemisphere, both in the coastal margin of the WES and in the oligotrophic gyre was very low. The C6 signal in the continental margin of the PAS was also low.

The distribution of the cumulative fluorescence intensity of humic-like components I_{Humic} in the meridional section followed the distribution of the $a_{CDOM}(305)$, with elevated values in the surface at northern and southern continental margins of the transect, strong depletion of I_{Humic} in the mixed layer in the northern and southern subtropical oligotrophic gyres and maximum values in the subsurface waters in the Equatorial Upwelling Zone (between 7 to 5° N at 50 m depth). There was evidence of advection of humic-like material between 20° N to 20° S associated with the equatorial upwelling. This was in contrast to the distribution of marine humic-like C5 that was strongly depleted in the surface layer (0 – 50 m depth) across all provinces except the PAS, where it reached a maximum.

The $I_{Protein}/I_{Humic}$ ratio is indicative of the contribution of the dominant fraction of DOM fluorescence: high values denote the dominance of protein-like components in the EEM array and low values indicate the dominance of the humic-like fraction. The highest values of $I_{Protein}/I_{Humic}$ were observed in the surface waters of the SATL; elevated values were also found in the mixed layer in the centre of the northern oligothrophic gyre. In the northern hemisphere, low values were found in the MLD and just below it with the lowest values at depths between 50 and 120 m in the EQU. In the southern hemisphere low values of $I_{Protein}/I_{Humic}$ were found below 200 m and in the mixed layer of the PAS. The $I_{Protein}/I_{Humic}$ indicated a shift in the DOM composition between northern and southern hemisphere waters. The relatively low fluorescence of the protein-like component in most of the samples (except the NAST-E) resulted in low ratios in these waters. The situation was reversed south of the 7°S where freshly produced DOM was dominated by the protein-like component and there was a lower fluorescence intensity of humic-like components. This resulted in maximum $I_{Protein}/I_{Humic}$ ratio in the SATL and protein-like components 15 times higher than humic-like components. Elevated values were also found at depths between 100 – 200 m between 10° S and 45° S.

3.5 *Relationships between DOM components and spectral indices of CDOM absorption and fluorescence and ocean water properties*.

The absorption spectrum slope coefficient, $S_{250\text{-}600}$, and spectral slope ratio, S_R, were linearly correlated with salinity. The fluorescence intensity of components C1 and C2, I_{C1} and

I_{C2}, were inversely correlated with salinity, (Figure 7). The percentage variability explained was highest between I_{C2} and salinity ($R^2 = 0.38$). The other parameters were weakly correlated with salinity, and the lowest percentage variability explained was between salinity and $a_{CDOM}(305)$; $R^2 = 0.14$ (data not shown). The intensity of individual protein-like components and cumulative intensity of the protein-like fraction of the EEMs were not correlated with salinity. Significant correlations at the $p<0.001$ confidence level for each relationship are given in the Table 5.

There were no significant trends between $a_{CDOM}(305)$, I_{Tot}, $I_{Protein}$, I_{C6} and temperature (data not shown). There was a weak positive relationship between the fluorescence intensity of protein-like components I_{C3} and I_{C4} and temperature, and an inverse relationship with low molecular weight autochthonous component I_{C5} (data not shown). Figure 8 gives the cumulative fluorescence intensity of humic-like components (I_{Humic}) and other indices against temperature in the upper 300 m. The negative linear trends between I_{Humic} and HIX and temperature and the positive linear trends between $S_{250\text{-}600}$, and S_R and temperature (Table 5), suggest that high molecular weight humic-like material is produced below the thermocline.

Figure 9 presents the distribution of the spectral slope coefficient, $S_{250\text{-}600}$, as a function of cumulative fluorescence of the humic fraction I_{Humic}. The highly significant inverse linear relationship between these parameters, ($R = 0.89$, $R^2 = 0.80$), suggests that the decomposition of the humic-like fraction in the mixed layer by photo-bleaching is mostly responsible for the loss of absorption in the visible part of the spectrum, which causes an increase in the steepness of $S_{250\text{-}600}$. The Humification Index is linearly related with fluorescence intensity humic-like fraction I_{Humic}. The inverse hyperbolic function was used to approximate empirical relationships between the HIX and $S_{250\text{-}600}$, and S_R. The coefficients calculated for those two relationships were low, but statistically significant.

4. Discussion.

The global distribution of the optical properties of CDOM based on *in situ* surveys is given in Nelson and Siegel, (2002), and Siegel et al., (2002, 2005a, 2005b). High $a_{CDOM}(\lambda)$ values were observed on the continental shelves and the upwelling areas of Mauritania and Chile. Very high values of $a_{CDOM}(\lambda)$ were reported by many authors close to the outlets of the major rivers e.g. Amazon River (Del Vecchio and Subramaniam, 2004), Congo River (Andrew et al., 2013) in the Atlantic Ocean, and Yangtze River in the Pacific Ocean

(Shanmugam, 2011). The central oligotrophic gyres of the Atlantic, Indian and Pacific oceans are extremely low in CDOM absorption. The zonal distribution of the Coloured Dissolved+Detrital Material, $a_{CDM}(440)$, at the surface presented by Siegel et al., (2002) indicated that highest values were observed in the polar waters of the Atlantic and Pacific Oceans in northern hemisphere and that $a_{CDM}(440)$ decreased significantly towards the subtropical gyres, with local maxima in the equatorial upwelling zone of all three oceans. The $a_{CDM}(440)$ dropped to a minimum in the subtropical gyres of the Global Ocean and then increased toward the Southern Ocean with clear demarcation of the subtropical and sub-polar frontal systems. This pattern has been confirmed by field surveys of $a_{CDOM}(\lambda)$in the Atlantic and Pacific Oceans (Nelson et al., 2007, Morel et al., 2007, Swan et al., 2009, Yamashita and Tanoue 2009, Bricaud et al., 2010). Kitidis et al. (2006) observed that subsurface $a_{CDOM}(300)$ maxima during AMT9-10 in 1999-2000, had the lowest spectral slopes and was associated with the DCM, suggesting a contribution of phytoplankton activity to CDOM production (Kitidis et al. 2006), though the samples were not filtered, so the signal may also be from particles. The strong depletion of CDOM in the surface waters, from 0–50 m, of the central oligotrophic gyres in the southern and northern hemispheres is the effect of the decomposition of CDOM due to photo-oxidation. In these waters exposure of CDOM trapped in the mixed layer to solar radiation and the high penetration of UV radiation due to the optical clarity of these waters can have a pronounced effect on the resulting $a_{CDOM}(300)$ values (Kitidis et al. 2006). The meridional distribution of the optical properties of CDOM in this study follows the global and regional patterns of $a_{CDOM}(\lambda)$ and S, also observed by Kitidis et al., (2006). The latitudinal and depth distribution of $a_{CDOM}(305)$ is determined by the salient oceanic circulation, the location of the subtropical, tropical and sub-polar fronts and the depth of the mixed layer.

The S_R, HIX, and FI have not been reported so far for the Atlantic Basin. The spectral indices that are quantitatively related to the composition, molecular weight, and state of the degradation of DOM provide a geographic signature for areas where transformation of DOM is high. These were mainly in the NAST-E and SATL, where S_R reached maxima and HIX index was at a minimum. These areas usually also had the highest spectral slope coefficients. The upper range in S_R was high (4.5), which have not been reported before. Originally Helm et al., (2008) reported that S_R values >2, in off shore regions of the Middle Atlantic Bight indicate that DOM has been transformed by both photo-degradation and bacterial uptake

546 processes. In the mixed layer of the NAST-E, we observed that S_R was >4, which suggests
547 high degradation of DOM. S_R values were lower in the mixed layer of the SATL compared to
548 the NAST-E, indicating differences in the molecular weight of DOM between the
549 oligotrophic gyres. The lower limit of the S_R was ca. 2, suggesting a low terrestrially derived
550 DOM input, which is characterized by $S_R \leq 1$ (Helms et al. 2008; Yamashita et al. 2010b).
551 Coincidentally HIX values were also very low in the mixed layer of oligotrophic
552 subtropical gyres, suggesting that DOM is mostly composed of low molecular weight
553 aliphatic dissolved organic compounds. The absolute variability in HIX was 0.28–5.15, and
554 the FI range was very small, from 1.01–1.29. Low values of HIX in open ocean samples
555 indicated low concentrations of terrestrial humic substances, which are characterized by
556 values from 10–16 (Zsolnay, at al., 1999). The maximum value of HIX corresponded to the
557 lowest dissolved oxygen values (Figure 2). This could indicate that microbial transformation
558 of DOM is a potential mechanism of humification in the open ocean. McKnight et al. (2001)
559 proposed that high values of FI (ca. 1.9) could be attributed to organic fluorophores produced
560 by bacteria, and that low values of FI (ca. 1.4) could be attributed to terrestrially derived
561 DOM fluorophores. We found that FI values were always <1.4, and never reached values
562 similar to those found in terrestrial systems, even for samples on the shelf margins. Similarly
563 low FI values (<1.4), have been reported for DOM/DOC rich tropical rivers of Venezuela
564 (Yamashita et al., 2010b) and a range of terrestrial aquatic ecosystems in the USA (Jaffé et
565 al., 2008). The FI values at coastal and estuarine sites in the US were usually >1.4 (Jaffé et al.,
566 2008). In contrast to these studies, the values we observed indicate that the spectral index is of
567 limited value for the determination of the source of DOM in pelagic ocean provinces.
568 The protein-like components are usually regarded as autochthonous and represent the
569 magnitude of the biological and microbial activity of the aquatic ecosystem. High abundance
570 of the protein-like fluorophores in oceanic waters may be expected based on previous studies
571 in diverse estuarine, marine and oceanic waters. Kowalczuk et al., (2003, 2009) for example
572 found a non-conservative mixing pattern of protein-like fluorophores in the salinity gradient
573 from the Cape Fear River outlet in Onslow Bay to the coastal zone. These were influenced by
574 optically clear Gulf Stream waters, which led to significant enrichment of DOM in coastal
575 waters with high protein-like substances relative to the humic-like fraction. Similar patterns
576 have also been observed by Kowalczuk et al., (2005) and Stedmon et al., (2007) in the Baltic
577 Sea. The non-conservative mixing of some protein-like and humic-like components has also

been observed in Japanese coastal waters (Yamashita at al., 2008) and Hudson Bay (Guéguen et al., 2011).

Humic-like components are usually highly correlated with salinity and their intensity decreases linearly with increasing salinity (see references cited above), indicating a predominant terrestrial source. Terrestrial humic-like components are diluted in oceanic water to 1.5% of the initial concentration compared to terrestrial aquatic environments (Murphy et al., 2008, Kowalczuk et al., 2009). Components C1 and C2 were also inversely related with temperature which suggests a basin-scale DOM re-mineralization as the source of the humic-like material found in the deep waters of the Atlantic Ocean, which can then be advected to the epipelagic layer, by upwelling. Humic-like components are also susceptible to photo-bleaching (Omori et al., 2011), which can cause a major reduction in them in the surface layer of the ocean. The vertical extent of the photo-degradation processes is limited to the penetration of the ultraviolet radiation in the ocean. In the tropical and subtropical zone the solar irradiance at the ultraviolet range (320 - 380 nm) may penetrate as deep as 80 m in the optically clearest waters of subtropical gyres (Morel et al., 2007; Smyth, 2011). The photo-degraded dissolved organic matter is trapped in the mixed layer and then re-circulated, which leads to the accumulation of degraded products (mainly low molecular weight DOM). The surface layer therefore becomes depleted of humic-like DOM components which may become mixed down to 200 m in the centre of subtropical gyres (Figure 6). The intensity of humic-like components in this study had a significant negative correlation with salinity (Figure 7, Table 5), that could reflect the mixing of terrestrially derived humic fraction of the DOM with oceanic water. This process is highly relevant at the continental margins of the transect, but in the pelagic open ocean, this may also be produced through the photodegradation of humic-like components in surface waters of the subtropical and tropical zone. Coincidently, the salinity in the subtropical gyres is highest due to high evaporation, and the optical signature of CDOM was extremely depleted at these locations. The production of humic-like compounds by microbial activity in the bathypelagic layer of the ocean has been observed in a number of studies (Yamashita and Tanoue 2004; Yamashita et al., 2010a; Jørgensen et al., 2011). These studies also report a significant positive correlation between humic-like components and AOU, a measure of microbial activity. AOU has also been found to be positively correlated with $a_{CDOM}(325)$, in intermediate and deep water masses of Atlantic, Pacific and Indian Oceans, (Nelson et al., 2007; Swan et al., 2009; Nelson et al., 2010). The vertical advection to mixed layer and latter degradation by photolysis may be indicative of the inverse relationship

between the fluorescence intensity of humic-like components and salinity. Jørgensen et al., (2011) proposed that the distribution of humic-like components in the ocean are in the steady state between supply from continental run off, local microbial production and photochemical removal in the surface layer. Our data support this mechanism of cycling of humic substances in the pelagic ocean. These findings are additionally supported by Opsahl and Benner, (1997) who used lignin biomarkers to estimate terrestrial DOM to be 0.7 – 2.4% of the bulk DOM found in the pelagic Atlantic and Pacific Oceans. The contribution of terrigenous DOM to bulk DOM is 3.6 times higher in the Atlantic compared to the Pacific Ocean, due to higher riverine discharge in the Atlantic Ocean. Opsahl and Benner, (1997) also found that terrigenous DOM is rapidly removed from the water column as a result of photochemical and microbial oxidation processes.

The maximum values of HIX, coincide with the maximum of the AOU, which was observed at depths >200 m from the Equator to 5°S. The regression of AOU against the fluorescence intensities of humic-like components I_{C1} and I_{C2} and cumulative fluorescence intensity of humic-like components $I_{Humic,}$ were statistically significant positive relationships (Figure 10). Data were restricted to samples collected at depths greater than 80-160 m (depending on the mixed layer depth at given location). The percentage variance explained was 0.66 for I_{C1}, 0.56 for I_{C2}, and 0.77 for I_{Humic}. The vertical distribution of DOM fluorescence components follow the general pattern in pelagic ocean presented by Stedmon and Álvarez-Salgado, (2011). There was an increase in the fluorescence intensity of protein-like components, mostly amino-acids, in the surface layer of oceanic waters, which then decreased sharply in the mesopelagic layer. There was a reversal in the pattern of the vertical distribution of fluorescence intensity humic-like substances, which was low in the surface layer and increased significantly in mesopelagic and bathypelagic layer of the open ocean. Regional and global studies have also confirmed these salient trends; for example Yamashita et al., (2007) reported low FDOM intensities in the surface waters, which in the Southern Ocean south off Tasmania and New Zealand, increased with depth. Similarly, Yamashita et al., (2010a) observed this pattern at four stations in the Okhotsk Sea and the northwestern North Pacific. Jørgensen et al., (2011) also observed these patterns in Atlantic, Pacific, Indian and Southern Oceans. The dominance of the protein-like components in the surface waters of the southern Canada Basin and in the East Siberia Sea was observed by Guéguen et al., (2012). The compositional differences in DOM fluorescence and the molecular weight distribution were observed in the Northern Pacific subtropical gyre by Omori et al., (2011),

644 who found low intensity of hydrophobic and bulk DOM fluorescence in the surface layer of
645 the gyre and increased fluorescence of both fractions in deeper layers. They also reported a
646 modification in the vertical distribution of DOM molecular weights, with lower molecular
647 weight substances in the surface and higher molecular weight substance in at deeper layers
648 (500 and 1000 m depth). Our data confirmed the overall dominance of protein-like
649 components in the composition of DOM in the mixed layer of the subtropical and tropical
650 zones of the Atlantic Ocean. The protein-like components form the largest proportion of the
651 total fluorescence intensity, which varied by depth along the transect. The maximum
652 fluorescence intensity of DOM was observed as a belt located between 100 and 200 m from
653 20°N to 40°S. The relative contribution of the protein-like components to the EEM array,
654 however, decreased sharply with depth and was not significant below the mixed layer. That
655 was also confirmed by the depth distribution of the HIX and $I_{Protein}/I_{Humic}$ (Figure 3, 6). There
656 was significant input of the humic-like components, presumably of terrestrial origin, from the
657 continental margin especially in the North Atlantic on the WES.
658 At the PAS, the contribution from humic-like components was lower, and there was a
659 higher contribution of protein-like components. In this area, the distribution of all components
660 and their mutual contribution to the bulk EEM intensity exhibited much less variability with
661 depth compared to other provinces of the Atlantic Ocean. The low levels of humic-like
662 components in the PAS and their relatively low humification (indicated by the low HIX
663 index), could be explained by a much lower discharge of fresh water into this region,
664 compared to the North Atlantic. The vertical distribution of almost all optical signature of
665 CDOM and DOM in the PAS was less variable, compared to the WES. This could be due to
666 differences in sampling between the northern and southern hemispheres during contrasting
667 seasons, especially with the onset of relatively weak thermal stratification at the beginning of
668 the austral spring in the PAS. Seasonal differences have previously been reported in the
669 optical properties of CDOM by Nelson et al., (1998) for the North Atlantic subtropical water
670 at the Bermuda Time Series site and by Omori et al., (2010) in the North Pacific subtropical
671 waters. The weakest vertical gradients in CDOM were found in the winter during deep mixing
672 events, and the largest were at the end of the summer, when there was a high degree of
673 thermal stratification and CDOM in the surface layer was degraded by photo-bleaching.
674 Differences in the phase of the seasonal cycle, succession of the phytoplankton
675 biomass and the exposure time to UV radiation in the mixed layer may also explain the higher
676 $I_{Protein}/I_{Humic}$ ratio, and lower SR and HIX values in the SATL compared to the

NAST-E. DOM trapped in the mixed layer in the NAST-E will have been exposed to sunlight for a longer duration than the DOM in the SATL, and DOM in the SATL will be of higher molecular weight due to deep water advection during winter mixing events. It could also be less degraded by photo bleaching due to a shorter exposure time to high doses of solar radiation. The freshly produced DOM by phytoplankton blooms in the SATL and PAS during austral spring, could contribute to a higher proportion of protein-like components in the surface waters. The smaller quantities of humic material, and lower intensities of humic-like components south of the Equator, would influence of $I_{\mathrm{Protein}}/I_{\mathrm{Humic}}$ ratio, also leading to an increase in the SATL.

5. Conclusions

Fluorescence Excitation Emission spectroscopy coupled with PARAFAC modeling was used to study the composition of the DOM in the Atlantic Ocean along a meridional transect. The analyses identified six DOM components: two humic-like components resulting from terrestrial run-off and microbial activity, one marine humic-like component and three protein-like components. Two of the protein-like components had spectral excitation and emission characteristics close to fluorescence properties of pure or bound amino acids, tyrosine and tryptophan. One of the protein–like components had an excitation and emission spectral characteristic that does not fit the spectral properties of known fluorescent amino acids which may arise from a combination of complex organic molecules of unknown origin. In our data set, the marine humic-like and protein-like components represent the autochthonous fraction of DOM, possibly released as phytoplankton exudates in all biogeographic provinces sampled during the cruise.

The DOM composition varied according to the dominant water masses in the biogeographic provinces. In all provinces except the North Atlantic Drift, protein-like compounds dominated the fluorescent DOM fraction in the mixed layer. The intensity of the humic-like components was depleted in the mixed layer especially in subtropical and tropical provinces. At the continental margins, humic-like components were only important at the Western European Shelf, probably due to significant run-off of humic-like material from terrestrial origin. Along the Patagonian Shelf, the humic-like components in the mixed layer were not significant, probably due to the smaller input of fresh water run-off into the South Atlantic compared to the North Atlantic. In all biogeographic provinces, there was a large shift in the DOM composition between waters below and in the mixed layer, with more humic and aromatic compounds characterized by a higher molecular weight in the mixed layer.

The humic-like fraction of DOM exhibited a significant negative correlation with salinity, and temperature and a positive correlation with Apparent Oxygen Utilization. These relationships indicated a net equilibrium between the supply of humic-like substances from the continental margins, in situ production by the microbial activity and photodegradation in the surface waters, especially in the subtropical and tropical regions. In this dataset, components C1 and C2 represent the allochtonous fraction of DOM, which presumably originate from different bacterial, viral and phytoplankton communities present in the biogeographic provinces sampled during the cruise. HIX was linearly correlated with the intensity of the humic-like DOM components and was non-linearly correlated with the qualitative indices of the CDOM absorption spectra and DOM fluorescence EEMs. HIX was also found to be an effective tool for delineating water masses of different DOM composition, areas of high microbial production of humic-like components and DOM degraded by solar UV radiation.

Acknowledgements: This study was supported by research grant no. 546/N-AMT-CDOM/2009/0 awarded to PK by the Polish National Science Centre. MZ participation in this study was supported by the SatBałtyk project funded by the European Union through the European Regional Development Fund, (contract No. POIG.01.01.02-22-011/09 entitled 'The Satellite Monitoring of the Baltic Sea Environment'). GT was supported by the Natural Environment Research Council UK National Capability, the Atlantic Meridional Transect. This is contribution number 229 to the AMT program. Comments by two anonymous reviewers greatly improved the manuscript.

References

Aiken J., N. Rees, S. Hooker, P. Holligan, A. Bale, D. Robins, G. Moore, R. Harris, and D. Pilgrim, 2000. The Atlantic Meridional Transect: overview and synthesis of data. Progress in Oceanography 45, 257–312.

Andersson, C. A., and R. Bro, 2000. The N-way toolbox for MATLAB. Chemometrics Intelligent Laboratory System 52, 1–4.

Andrew A. A., R. Del Vecchio, A. Subramaniam, and N. V. Blough, 2013. Chromophoric dissolved organic matter (CDOM) in the Equatorial Atlantic Ocean: Optical properties and their relation to CDOM structure and source. Marine Chemistry 148, 33–43.

Astoreca, R., V. Rousseau and C. Lancelot, 2009. Coloured dissolved organic matter (CDOM) in Southern North Sea waters: Optical characterization and possible origin. Estuarine, Coastal and Shelf Science 85, 633–640.

Blough, N. V., and R. Del Vecchio, 2002. Chromophoric DOM in the coastal environment. In: Hansell, D., Carlson, C. (Eds.), Biogeochemistry of Marine Dissolved Organic Matter. Academic Press, New York, pp. 509–546.

Benner, R., 2002. Chemical composition and reactivity. In: Hansell, C., Carlson (Eds.), Biogeochemistry of Marine Dissolved Organic Matter. Academic Press, New York, pp. 59–90.

751 Bricaud, A., M. Babin, H. Claustre, J. Ras, and F. Tièche, 2010. Light absorption properties
752 and absorption budget of Southeast Pacific waters. Journal of Geophysical Research
753 115, C08009, doi:10.1029/2009JC005517.
754 Carder, K.L., Steward, R.G., Harvey, G.R., Ortner, P.B.,1989. Marine humic and fulvic acids.
755 Their effect on remote sensing of ocean chlorophyll. Limnology and Oceanography 34,
756 68–81.
757 Coble, P. G., 1996. Characterization of marine and terrestrial DOM in seawater using
758 excitation–emission matrix spectroscopy. Marine Chemistry 51, 325–346.
759 Del Vecchio, R., and A. Subramaniam, 2004. Influence of the Amazon River on the surface
760 optical properties of the western tropical North Atlantic Ocean. Journal of Geophysical
761 Research 109, C11001, doi:10.1029/2004JC002503.
762 Duursma, E.K., 1974. The fluorescence of dissolved organic matter in the sea. In: Jerlov,
763 N.G., Steeman Nielsen, E. (Eds.), Optical Aspects of Oceanography. Academic Press,
764 New York, pp. 237–256.
765 D'Sa, E. J., R. G. Steward, A. Vodacek, N. V. Blough and D. Phinney, 1999. Determining
766 optical absorption of colored dissolved organic matter in seawater with a liquid
767 capillary waveguide. Limnology and Oceanography, 44:1142-1148.
768 Ferrari, G., 2000. The relationship between chromophoric dissolved organic matter and
769 dissolved organic carbon in the European Atlantic coastal area and in the West
770 Mediterranean Sea (Gulf of Lions). Marine Chemistry 70 (4), 339–357.
771 Ferrari, G., and M. Dowell, 1998. CDOM absorption characteristics with relation to
772 fluorescence and salinity in coastal areas of the southern Baltic Sea. Estuarine Coastal
773 and Shelf Science 47 (1), 91–105.
774 Guéguen C. and C.W. Cuss 2011. Characterisation of aquatic dissolved organic matter by
775 asymmetrical flow field-flow fractionation coupled to UV-Visible diode array and
776 excitation emission matrix fluorescence. Journal of Chromatography A, 1218, 4188-
777 2198.
778 Guéguen, C., M. A. Granskog, G. McCullough, and D. G. Barber, 2011. Characterisation of
779 colored dissolved organic matter in Hudson Bay and Hudson Strait using parallel factor
780 analysis. Journal of Marine Systems 88, 423–433.
781 Guéguen, C., F. A. McLaughlin, E. C. Carmack, M. Itoh, H. Narita, and S. Nishino, 2012.
782 The nature of colored dissolved organic matter in the southern Canada Basin and East
783 Siberian Sea. Deep-Sea Research II, (81–84), 102–113.
784 Hansell, D.A., 2013. Recalcitrant Dissolved Organic Carbon Fractions. Annual Review of
785 Marine Science, 5: 421-445.
786 Harvey, G.R., Boran, D.A., Chesal, L.A., Tokar, J.M., 1983. The structure of marine fulvic
787 and humic acids. Marine Chemistry 12, 119–132.
788 Hedges, J. I., 2002. Why dissolved organic matter. In: Hansell, D., Carlson, C. (Eds.),
789 Biogeochemistry of Marine Dissolved Organic Matter. Academic Press, New York, pp.
790 1–33.
791 Helms, J. R., A. Stubbins, J. D. Ritchie, E. C. Minor, D. J. Kieber and K. Mopper, 2008.
792 Absorption spectral slopes and slope ratios as indicators of molecular weight, source,
793 and photobleaching of chromophoric dissolved organic matter. Limnology and
794 Oceanography, 53(3), 955–969.
795 Hoge, F. E., R. N. Swift, J. K. Yungel, and A. Vodacek, 1993. Fluorescence of dissolved
796 organic matter: a comparison of North Pacific and North Atlantic Oceans during April
797 1993. Journal of Geophysical Research 98, 22779–22787.

Jaffé, R., D. McKnight, N. Maie, R. Cory, W. H. McDowell, and J. L. Campbell, 2008. Spatial and temporal variations in DOM composition in ecosystems: The importance of long-term monitoring of optical properties. Journal of Geophysical Research 113, G04032, doi:10.1029/2008JG0006.

Jerlov, N.G., 1976. Marine Optics. Elsevier, New York. 231 pp.

Jiao, N., F. Azam, and S. Sanders, (Eds.), 2011. Microbial carbon pump in the ocean. American Association for the Advancement of Science, Washington, DC, 2011, 72 pp.

Jørgensen, L., C. A. Stedmon, T. Kragh, S. Markager, M. Middelboe, and M. Søndergaard, 2011. Global trends in the fluorescence characteristics and distribution of marine dissolved organic matter. Marine Chemistry 126. 139–148.

Kowalczuk, P., W. J. Cooper, R. F. Whitehead, M. J. Durako and W. Sheldon, 2003. Characterization of CDOM in organic rich river and surrounding coastal ocean in the South Atlantic Bight. Aquatic Sciences 65(4), 384-401.

Kowalczuk P., J. Stoń-Egiert, W. J. Cooper, R. F. Whitehead, and M. J. Durako, 2005. Characterization of Chromophoric Dissolved Organic Matter (CDOM) in the Baltic Sea by Excitation Emission Matrix fluorescence spectroscopy. Marine Chemistry, 96, 273-292.

Kowalczuk P., C. A. Stedmon and S. Markager, 2006. Modeling absorption by CDOM in the Baltic Sea from season, salinity and chlorophyll. Marine Chemistry 101, 1–11.

Kowalczuk, P., M. J. Durako, H. Young, A. E. Kahn, W. J. Cooper and M. Gonsior, 2009. Characterization of dissolved organic matter fluorescence in the South Atlantic Bight with use of PARAFAC model: Interannual variability Marine Chemistry 113, 182-196.

Kitidis, V., A. P. Stubbins, G. Uher, R. C. Upsill Goddard, C. S. Law and E. M. S. Woodward, 2006. Variability of Chromophoric Organic Matter in surface waters of the Atlantic Ocean. Deep Sea Research II, 53, 1666-1684.

Longhurst A., 1995. Seasonal cycles of pelagic production and consumption. Progress in Oceanography, 36, 77-167.

McKnight, D. M., E. W. Boyer, P. K. Westerhoff, P. T. Doran, T. Kulbe, D. T. Andersen, 2001. Spectrofluorometric characterization of dissolved organic matter for indication of precursor organic material and aromaticity. Limnology and Oceanography, 46(1), 38–48.

Miller, R. L., M. Belz, C. Del Castillo, and R. Trzaska, 2002. Determining CDOM absorption spectra in diverse coastal environments using a multiple pathlength, liquid core waveguide system. Continental Shelf Research, 22:1301-1310.

Moens, P. E., M. K. Helms, and D. M. Jameson, 2004. Detection of tryptophan to tryptophan energy transfer in proteins. The Protein Journal 23. 79–83.

Morel A., B. Gentili, H. Claustre, M. Babin, A. Bricaud, J. Ras, and F. Tièche, 2007. Optical properties of the ‘‘clearest’’ natural waters. Limnology and Oceanography 52(1), 217–229.

Murphy, K. R., K. D. Butler, R. G. M. Spencer, C. A. Stedmon, J. R. Boehme and G. R. Aiken, 2010. Measurement of Dissolved Organic Matter Fluorescence in Aquatic Environments: An Interlaboratory Comparison. Environmental Science and Technology, 44, 9405–9412.

Murphy, K. R., G. M. Ruiz, W. T. M. Dunsmuir, and T. D. Waite, 2006. Optimized parameters for fluorescence-based verification of ballast water exchange by ships. Environmental Science and Technology 40 (7), 2357–2362.

Murphy. K. R., C. A. Stedmon, T. D. Waite, and G. M. Ruiz, 2008. Distinguishing between terrestrial and autochthonous organic matter sources in marine environments using fluorescence spectroscopy. Marine Chemistry 108, 40-58.

Nelson N. B., and D. A. Siegel, 2002. Chromophoric DOM in the open ocean. In: Hansell, D. A., Carlson, C. A. (Eds.). Biogeochemistry of Marine Dissolved Organic Matter. Academic Press, San Diego, CA., 547–578.

Nelson N. B., and D. A. Siegel, 2013. The Global Distribution and Dynamics of Chromophoric Dissolved Organic Matter. Annual Review of Marine Science, 5, 447–476.

Nelson. N .B., D. A. Siegel, and A. F. Michaels, 1998. Seasonal dynamics of colored dissolved material in the Sargasso Sea. Deep Sea Research I 45. 931–957.

Nelson N. B., D. A. Siegel, C. A. Carlson, C. Swan, W. M. Smethie and S. Khatiwala, 2007. Hydrography of chromophoric dissolved organic matter in the North Atlantic. Deep-Sea Research I, 54.710–731.

Nelson. N. B.. D. A. Siegel. C. A. Carlson. and C. Swan, 2010. Tracing global biogeochemical cycles and meridional overturning circulation using chromophoric dissolved organic matter. Geophysical Research Letters 37 L03610. doi:10.1029/2009GL042325.

Omori, Y., T. Hama, M. Ishii, and S. Saito, 2010. Relationship between the seasonal change in fluorescent dissolved organic matter and mixed layer depth in the subtropical western North Pacific. Journal of Geophysical Research 115, C06001, doi:10.1029/2009JC005526.

Omori, Y., T. Hama, M. Ishii, and S. Saito, 2011. Vertical change in the composition of marine humic-like fluorescent dissolved organic matter in the subtropical western North Pacific and its relation to photoreactivity. Marine Chemistry 124, 38–47.

Opsahl, S., Benner, R., 1997. Distribution and cycling of terrigenous dissolved organic matter in the ocean. Nature 386, 480–482.

Robinson, C., Alex J. Poulton, P. M. Holligan, A. R. Baker, G. Forster, N. Gist, T. D. Jickells, G. Malin, R. Upstill-Goddard, R. G. Williams, E. M. S. Woodward, and M. V. Zubkov, 2006. The Atlantic Meridional Transect (AMT) Programme: A contextual view 1995–2005. Deep-Sea Research II 53, 1485–1515.

Romera-Castillo, C., H. Sarmento, X. A. Álvarez-Salgado, J. M. Gasol, and C. Marrasé, 2010. Production of chromophoric dissolved organic matter by marine phytoplankton. Limnology and Oceanography, 55(1), 446–454.

Romera-Castillo, C., H. Sarmento, X. A. Álvarez-Salgado, J. M. Gasol, and C. Marrasé, 2011. Net production and consumption of fluorescent Colored Dissolved Organic Matter by natural bacterial assemblages growing on marine phytoplankton exudates. Applied and Environmental Microbiology, 7490–7498.

Shanmugam, P. 2011. New models for retrieving and partitioning the colored dissolved organic matter in the global ocean: Implications for remote sensing. Remote Sensing of Environment 115, 1501–1521.

Siegel, D. A., S. Maritorena, N. B. Nelson, D. A. Hansell, M. Lorenzi-Kayser, 2002.Global ocean distribution and dynamics of colored dissolved and detrital organic materials. Journal of Geophysical Research 107(C12), 3228, doi:10.1029/2001JC000965.

Siegel, D. A., S. Maritorena, N. B. Nelson, and M. J. Behrenfeld, 2005a. Independence and interdependencies among global ocean color properties: Reassessing the bio-optical

890 assumption. Journal of Geophysical Research, 110, C07011,
891 doi:10.1029/2004JC002527
892 Siegel, D. A., S. Maritorena, N. B. Nelson, M. J. Behrenfeld, and C. R. McClain, 2005b.
893 Colored dissolved organic matter and its influence on the satellite-based
894 characterization of the ocean biosphere, Geophysical Research Letters 32, L20605,
895 doi:10.1029/2005GL024310.
896 Smyth, T. J., 2011. Penetration of UV irradiance into the global ocean. Journal of
897 Geophysical Research 116, C11020, doi:10.1029/2011JC007183.
898 Stedmon, C. A., and X. A. Álvarez-Salgado, 2011. Shedding Light on a Black Box: UV-
899 Visible spectroscopic characterization of marine Dissolved Organic Matter. [in:] N.
900 Jiao, F. Azam, and S. Sanders, eds. Microbial carbon pump in the ocean. American
901 Association for the Advancement of Science, Washington, DC, 2011, 62-63.
902 Stedmon, C. A., and R. Bro, 2008. Characterizing dissolved organic matter fluorescence with
903 parallel factor analysis: a tutorial. Limnology and Oceanography: Methods 6, 572–579.
904 Stedmon C. A., and S. Markager, 2003. Behaviour of the optical properties of coloured
905 dissolved organic matter under conservative mixing. Estuarine, Coastal and Shelf
906 Science 57, 973–979.
907 Stedmon C. A., and S. Markager, 2005a. Resolving the variability in dissolved organic matter
908 fluorescence in a temperate estuary and its catchment using PARAFAC analysis.
909 Limnology and Oceanography 50(5), 686-697.
910 Stedmon C. A., and S. Markager, 2005b. Tracing the production and degradation of
911 autochthonous fractions of dissolved organic matter by fluorescence analysis.
912 Limnology and Oceanography, 50(5) 1415-1426.
913 Stedmon, C.A., S. Markager and R. Bro, 2003. Tracing dissolved organic matter in aquatic
914 environments using a new approach to fluorescence spectroscopy. Marine Chemistry
915 82, 239–254.
916 Stedmon, C. A., S. Markager and H. Kaas, 2000. Optical Properties and Signatures of
917 Chromophoric Dissolved Organic Matter (CDOM) in Danish Coastal Waters. Estuarine
918 Coastal and Shelf Science, 51, 267–278.
919 Stedmon, C. A., S. Markager, L. Tranvik, L. Kronberg, T. Slätis, and W. Martinsen, 2007.
920 Photochemical production of ammonium and transformation of dissolved organic matter
921 in the Baltic Sea. Marine Chemistry 104, 227–240.
922 Stedmon C. A., C. L. Osburn and T. Kragh, 2010. Tracing water mass mixing in the Baltic–
923 North Sea transition zone using the optical properties of coloured dissolved organic
924 matter. Estuarine, Coastal and Shelf Science 87, 156–162.
925 Stubbins, A., G. Uher, V. Kitidis, C. S. Law, R. C. Upstill-Goddard, E. M. S. Woodward,
926 2006. The open-ocean source of atmospheric carbon monoxide. Deep-Sea Research II
927 53, 1685–1694.
928 Sulzberger, B. and E. Durisch-Kaiser, 2009. Chemical characterization of dissolved organic
929 matter (DOM): A prerequisite for understanding UV-induced changes of DOM
930 absorption properties and bioavailability. Aquatic Sciences 71, 104-126.
931 Swan C. M., D. A. Siegel, N. B. Nelson, C. A. Carlson and E. Nasir, 2009. Biogeochemical
932 and hydrographic controls on chromophoric dissolved organic matter distribution in the
933 Pacific Ocean. Deep Sea Research Part I 56, 2175–2192.
934 Swan C. M., N. B. Nelson, D. A. Siegel, and E. A. Fields, 2013. A model for remote
935 estimation of ultraviolet absorption by chromophoric dissolved organic matter based on
936 the global distribution of spectral slope. Remote Sensing of Environment 136, 277–285.

Tedetti, M., B. Charriére, A. Bricaud, J. Para, P. Raimbault, and R. Sempére, 2010. Distribution of normalized water-leaving radiances at UV and visible wave bands in relation with chlorophyll a and colored detrital matter content in the southeast Pacific. Journal of Geophysical Research 115, C02010, doi:10.1029/2009JC005289.

Twardowski, M.S., and P. L. Donaghay, 2002. Photobleaching ofaquatic dissolved materials: absorption removal, spectral alteration, and their interrelationship. Journal of Geophysical Research, 107 (C8), doi: 10.1029/1999JC000281.

Vähätalo, A.V., Zepp, R.G., 2005. Photochemical mineralisation of dissolved organic nitrogen to ammonium in the Baltic Sea. Environmental Science and Technology 39, 6985–6992.

Vodacek, A., N. V. Blough, M. D. DeGrandpre, E. T. Peltzer, and R. K. Nelson, 1997. Seasonal variation of CDOM and DOC in the Middle Atlantic Bight: terrestrial inputs and photooxidation. Limnology and Oceanography 42 (2), 674–686.

Yamashita Y., and E. Tanoue, 2004. In situ production of chromophoric dissolved organic matter in coastal environments. Geophysical Research Letters 31, L14302, doi:10.1029/2004GL019734.

Yamashita Y., and E. Tanoue, 2009. Basin scale distribution of chromophoric dissolved organic matter in the Pacific Ocean. Limnology and Oceanography 54(2), 598–609.

Yamashita Y., R. M. Cory, J. Nishioka, K. Kuma, E. Tanoue, and R. Jaffé, 2010a. Fluorescence characteristics of dissolved organic matter in the deep waters of the Okhotsk Sea and the northwestern North Pacific Ocean. Deep Sea Research Part II 57, 1478-1485.

Yamashita, Y., R. Jaffé, N. Maie, and E. Tanoue, 2008. Assessing the dynamics of dissolved organic matter (DOM) in coastal environments by excitation emission matrix fluorescence and parallel factor analysis (EEM-PARAFAC). Limnology and Oceanography 53(5), 1900–1908.

Yamashita, Y., N. Maie, H. Briceño, and R. R. Jaffé, 2010b. Optical characterization of dissolved organic matter in tropical rivers of the Guayana Shield, Venezuela, Journal of Geophysical Research 115, G00F10, doi:10.1029/2009JG000987.

Yamashita Y., A. Tsujasaki, T. Nishida and E. Tanoue 2007.Vertical and horizontal distribution of fluorescent dissolved organic matter in the Southern Ocean. Marine Chemistry 106, 498-509.

Zsolnay, A., E. Baigar, M. Jimenez, B. Steinweg, and F. Saccomandi, 1999. Differentiating with fluorescence spectroscopy the sources of Dissolved Organic Matter in soils subjected to drying. Chemosphere 38(1), 45-50.

973 Figures captions

974 Figure 1. Location of sampling stations along the AMT 20 cruise track overlain on boundaries
975 of bio-geographic provinces according to Longhurst (1995).

976 Figure 2. Meridional sections of Absolute Salinity (S_A), temperature, chlorophyll-*a*
977 fluorescence and Apparent Oxygen Utilization. The solid line overlaid on the section
978 plots represents the depth of the thermocline. The vertical line delineates boundaries of
979 Longhurst (1995) biogeographic provinces.

980 Figure 3. Meridional sections of the distribution of CDOM absorption coefficient,
981 $a_{CDOM}(305)$, spectral slope coefficient, $S_{250\text{-}600}$, and spectral slope ratio, S_R and
982 Humification Index – HIX. The solid line overlaid on the section plots represents the
983 depth of the thermocline. The vertical line delineates boundaries of Longhurst (1995)
984 biogeographic provinces.

985 Figure 4. The PARAFAC model output showing fluorescence signatures of six components
986 identified in the AMT20 data set. Contour plots present spectral shapes of excitation
987 and emission of derived components. Components C1–C6 are ordered by decreasing
988 percent of explained variation. Line plots at right side of each contour plot present split-
989 half validation results for each identified component. Excitation (left) and emission
990 (right) spectra were estimated from three independent 6-component PARAFAC models
991 run on two random halves of the data set (CAL — blue lines, VAL — green lines) and
992 the complete data set (red lines).

993 Figure 5. Composition of CDOM fluorescence excitation and emission matrix spectra in the
994 mixed (upper graph) and below mixed layer (lower graph) in major biogeographic
995 provinces of the Atlantic Ocean: WES - Western European Shelf, NAST(E) - North
996 Atlantic Subtropical Gyre, EQU - Equatorial Upwelling, SATL - South Atlantic
997 Subtropical Gyre, PAS - Patagonian Shelf. Bar plots represent average intensity of 6
998 components calculated for samples collected at a particular province and the depth
999 range, the whisker represents the standard deviation.

1000 Figure 6. Meridional sections of the distribution of total DOM fluorescence intensity, I_{Tot},
1001 intensity of the humic fraction of the DOM fluorescence, I_{Humic}, intensity of the protein-
1002 like fraction of the DOM fluorescence, $I_{Protein}$ and the ratio of respective DOM
1003 fluorescence fractions, $I_{Protein}/I_{Humic}$. The solid line overlaid on the section plots
1004 represents the depth of the thermocline. The vertical line delineates boundaries of
1005 Longhurst (1995) biogeographic provinces.

1006 Figure 7. Relationships of the salinity and spectral slope coefficient, $S_{250\text{-}600}$, spectral slope
1007 ratio S_R, and fluorescence intensity of components C1 and C2, I_{C1}, I_{C2}, during the
1008 AMT20 cruise.

1009 Figure 8. Distribution of the fluorescence intensity of humic like components I_{Humic},
1010 humification index, HIX, spectral slope coefficient, $S_{250\text{-}600}$, and the spectral slope ratio
1011 S_R, in the function of water temperature during the AMT20 cruise.

Figure 9. Relationships between fluorescence intensity of humic-like components, I_{Humic}, and spectral slope coefficient, $S_{250\text{-}600}$ (upper left panel). Relationships between Humification Index, HIX, and fluorescence intensity of humic-like components, I_{Humic}, spectral slope coefficient, $S_{250\text{-}600}$, and spectral slope ratio S_R.

Figure 10. Relationship between Apparent Oxygen Utilization and the cumulative fluorescence intensity of humic-like components I_{Humic} in the Atlantic Ocean over the depth range of 140-300 m.

1021 Table 1 Average and standard error $a_{CDOM}(305)$, $S_{250–600}$, S_R, and fluorescence spectral
1022 indexes, FI and HIX values in significant biogeographic provinces sampled during
1023 AMT20 cruise (October – November 2010).

Province		$a_{CDOM}(305)$ [m^{-1}]	$S_{250–600}$ [nm^{-1}]	S_R	FI	HIX
European Continental Shelf Waters	Mixed layer	0.39±0.033	0.026±0.0006	2.39±0.07	1.14±0.005	1.80±0.043
	Below Mixed layer	0.27±0.028	0.028±0.0006	2.69±0.10	1.17±0.01	2.78±0.220
North Atlantic Subtropical Gyre	Mixed layer	0.19±0.009	0.034±0.0006	3.42±0.10	1.16±0.006	0.88±0.069
	Below mixed layer	0.24±0.007	0.028±0.0002	2.86±0.04	1.19±0.022	2.45±0.010
Equatorial Upwelling	Mixed layer	0.20±0.009	0.034±0.0005	2.99±0.10	1.14±0.021	0.92±0.123
	Below mixed layer	0.31±0.015	0.023±0.0005	2.40±0.04	1.20±0.035	2.77±0.298
South Atlantic Subtropical Gyre	Mixed layer	0.17±0.005	0.034±0.0004	3.26±0.06	1.17±0.007	0.66±0.052
	Below mixed layer	0.23±0.009	0.027±0.0007	2.70±0.07	1.22±0.038	2.60±0.256
Patagonian Shelf	Mixed layer	0.28±0.016	0.027±0.0008	2.58±0.09	1.12±0.006	1.37±0.111
	Below mixed layer	0.22±0.004	0.028±0.001	2.93±0.04	1.17±0.021	1.57±0.143
All data	Mixed layer	0.22±0.009	0.032±0.0004	3.09±0.05	1.15±0.004	0.97±0.050
	Below mixed layer	0.25±0.005	0.027±0.0003	2.75±0.03	1.19±0.032	2.40±0.094

1024

1025

Table 2. Spectral characteristics of excitation and emission maxima of six components identified by PARAFAC modeling for the whole EEMs data set collected in the Atlantic Ocean during AMT20 cruise compared to previously identified sources. Secondary excitation bands are given in brackets.

Component no.	Excitation maximum	Emission maximum	Coble (1996)	Description and probable source
1	240/(320) nm	396 nm	A peak 260/380-460	Terrestrial humic-like substances Component 1: 240/436 (Ref. 1) Component 1: 250/448 (Ref. 3) Component 1: 250/458 (Ref. 6)
2	240(370) nm	480 nm	A peak 260/380-460 C peak 350/420-480	Terrestrial humic- like substances. widespread. Component 3: 270 (360)/478 (Ref. 1) Component 2: 250 (385)/504 (Ref. 3) Component 3: 260(370)/490 (Ref. 5)
3	270 nm	348 nm		Presumably combined fluorescence of the free amino acids: phenylalanine, tryptophan and tyrosine, or bound in proteins. Component 6, (Ref. 7)
4	275 nm	300 nm	B peak 275/305	Amino acids. free or bound in proteins Tyrosine: 275/310 (Ref. 6) Component 8: 275/304 (Ref. 3) Component 4: 275/306 (Ref. 4) Component 1: 275/300 (Ref. 5) Component 7: 270/299 (Ref. 6)
5	300 nm	408 nm	M peak 312/380-420	Marine and terrestrial humic materials. possible microbial reprocessing. Terrestrial component 4: (250) 325/416 (Ref. 1) Microbial component 3: 295/398 (Ref. 4) Component 2: 315/418 (Ref. 5) Component 6: 325/385 (Ref. 6)
6	295 nm	334(360) nm	T peak 275/340	Amino acids, free or bound in proteins Tryptophan: 278/340 (Ref. 2) Component 6: 280/338 (Ref. 4) Component 7: 280/344 (Ref. 3) Component 6: 280/328 (Ref. 5) Component 4: 280/318 (Ref. 6)

Ref. 1 – Stedmon et al., (2003), Ref. 2 – Kowalczuk et al., (2003), Ref. 3 – Stedmon and Markager (2005a), Ref. 4 – Stedmon and Makager (2005b), Ref. 5 – Murphy et al., (2008), Ref. 6 – Yamashita et al., (2008), Ref. 7 – Jørgensen et al., (2011).

Table 3. One Way Analysis of variance for $a_{CDOM}(305)$, $S_{250–600}$ S_R, FI, HIX, fluorescence intensity of all components identified by PARAFAC model, and cumulative fluorescence of protein-like components, $I_{Protein}$, cumulative fluorescence of humic-like components, I_{Hum}, and their mutual ratio, $I_{Protein}/I_{Hum}$, by depth and by province during AMT20 cruise.

Parameter		*N*	F	P	Highest	Lowest
$a_{CDOM}(305)$	Mixed layer	204	0.14	0.706	NS	NS
	Province	204	17.63	<0.0001	WES	SATL
$S_{250–600}$	Mixed layer	204	58.76	<0.0001	MLD	Below MLD
	Province	204	8.0	<0.0001	NAST, SATL	PAS
S_R	Mixed layer	203	24.70	<0.0001	MLD	Below MLD
	Province	203	14.52	<0.0001	NAST, SATL	WES
FI	Mixed layer	201	56.63	<0.0001	Below MLD	MLD
	Province	201	6.88	<0.0001	SATL	WES, PAS
HIX	Mixed layer	201	198.92	<0.0001	Below MLD	MLD
	Province	201	4.19	0.003	WES	SATL
I_{C1}	Mixed layer	201	271.40	<0.0001	Below MLD	MLD
	Province	201	5.29	<0.0001	EQU, WES	SATL
I_{C2}	Mixed layer	201	137.12	<0.0001	Below MLD	MLD
	Province	201	10.76	<0.0001	WES, EQU	SATL
I_{C3}	Mixed layer	201	41.16	<0.0001	MLD	Below MLD
	Province	201	3.19	0.014	WES	NAST
I_{C4}	Mixed layer	201	2.78	0.097	NS	NS
	Province	201	6.02	<0.0001	SATL, EQU, PAS	WES
I_{C5}	Mixed layer	201	72.15	<0.0001	Below MLD	MLD

	Province	201	4.79	0.001	EQU	NAST
I_{C6}	Mixed layer	201	1.86	0.174	NS	NS
	Province	201	22.67	<0.0001	SATL, EQU	NAST
I_{tot}	Mixed layer	201	15.58	<0.0001	Below MLD	MLD
	Province	201	8.38	<0.0001	EQU	NAST
I_{Hum}	Mixed layer	201	220.14	<0.0001	Below MLD	MLD
	Province	201	7.11	<0.0001	WES, EQU	SATL
$I_{Protein}$	Mixed layer	201	8.15	0.005	MLD	Below MLD
	Province	201	8.10	<0.0001	EQU, SATL, PAS	WES, NAST
$I_{Protein}/I_{Hum}$	Mixed layer	201	134.24	<0.0001	MLD	Below MLD
	Province	201	9.14	<0.0001	SATL	WES

Table 4. Average and standard deviation of fluorescence intensity of respective components in major biogeographic provinces of Atlantic Ocean, in the mixed layer and below it, identified by PARAFAC model in samples collected during AMT 20 cruise.

Province		I_{C1} [R.U.]	I_{C2} [R.U.]	I_{C3} [R.U.]	I_{C4} [4 R.U.]	I_{C5} [R.U.]	I_{C6} [R.U.]
European Continental Shelf Waters	Mixed layer	0.0115±0.0055	0.0087±0.0034	0.0131±0.0045	0.0099±0.0090	0.0095±0.0070	0.0071±0.0019
	Below Mixed Layer	0.0134±0.0005	0.0089±0.0005	0.0107±0.0064	0.0031±0.0023	0.0085±0.0010	0.0067±0.0017
North Atlantic Subtropical Gyre	Mixed layer	0.0046±0.0020	0.0032±0.0014	0.0098±0.0027	0.0136±0.013	0.0048±0.0024	0.0058±0.0014
	Below Mixed Layer	0.0131±0.0024	0.0079±0.0017	0.0081±0.0024	0.0111±0.0117	0.0092±0.00235	0.0060±0.0022
Equatorial Upwelling	Mixed layer	0.0056±0.0019	0.0044±0.0011	0.0122±0.0043	0.0194±0.0198	0.0076±0.0052	0.01102±0.0063
	Below Mixed Layer	0.0193±0.0021	0.0110±0.0018	0.0088±0.0041	0.0187±0.0206	0.0128±0.0024	0.0097±0.0041
South Atlantic Subtropical Gyre	Mixed layer	0.0043±0.0020	0.0028±0.0012	0.0115±0.0032	0.0196±0.0152	0.0062±0.0028	0.01098±0.0050
	Below Mixed Layer	0.0149±0.0035	0.0082±0.0029	0.0067±0.0025	0.0154±0.01215	0.0117±0.0027	0.0104±0.0048
Patagonian Shelf	Mixed layer	0.0080±0.0027	0.0069±0.0023	0.0116±0.0026	0.0160±0.0172	0.0092±0.0040	0.0075±0.0015
	Below Mixed Layer	0.0098±0.0016	0.0063±0.0005	0.0099±0.0043	0.0201±0.0207	0.0104±0.0040	0.0070±0.0024
All data	Mixed layer	0.0058±0.0036	0.0043±0.0027	0.01121±0.0034	0.0160±0.0148	0.0066±0.0041	0.0084±0.0043
	Below Mixed Layer	0.0138±0.0037	0.0082±0.0023	0.0084±0.0036	0.0141±0.0153	0.0104±0.0030	0.0078±0.0037

Table 5. Results of regression analysis among salinity, spectral slope coefficient $S_{250\text{-}600}$, spectral slope ratio S_R, and fluorescence intensity of components C1 and C2, I_{C1}, I_{C2}. Results of regression analysis among temperature and fluorescence intensity of humic like pigments, I_{Hum}, humification index, HIX, spectral slope, $S_{250\text{-}600}$, and spectral slope ratio, S_R. Results of regression analysis between spectral slope, $S_{250\text{-}600}$, and fluorescence intensity of humic like pigments, I_{Hum}, and among humification index HIX and fluorescence intensity of humic like pigments, I_{Hum}, spectral slope, $S_{250\text{-}600}$, and spectral slope ratio, S_R.

Parameters	Equation type	Regression coefficients	R	R^2	Sample size
Salinity vs. $S_{250\text{-}600}$	Linear y = a*x + b	a = 0.004 ± 0.0003 b = -0.101 ± 0.010	0.66	0.44	204
Salinity vs. S_R	Linear y = a*x + b	a = 0.367 ± 0.032 b = -10.287 ± 1.155	0.63	0.39	204
Salinity vs. I_{C1}	Linear y = a*x + b	a = - 0.003 ± 0.0004 b = 0.123 ± 0.015	0.47	0.22	202
Salinity vs. I_{C2}	Linear y = a*x + b	a = - 0.002 ± 0.0002 b = 0.094 ± 0.008	0.61	0.38	202
Temperature vs. I_{Humic}	Linear y = a*x + b	a = - 0.0010 ± 0.0001 b = 0.0342 ± 0.0015	0.66	0.43	202
Temperature vs. HIX	Linear y = a*x + b	a = -0.1203 ± 0.0095 b = 3.9386 ± 0.1855	0.67	0.44	202
Temperature vs. $S_{250\text{-}600}$	Linear y = a*x + b	a = 0.0006 ± 0.0001 b = 0.0187 ± 0.0007	0.78	0.61	202
Temperature vs. S_R	Linear y = a*x + b	a = 0.0473 ± 0.0047 b = 2.0423 ± 0.0911	0.58	0.34	202
I_{Humic} vs. $S_{250\text{-}600}$	Linear y = a*x + b	a = -0.462 ± 0.0166 b = 0.0373 ± 0.0003	0.89	0.80	202
HIX vs. I_{Hum}	Linear y = a*x + b	a = 0.0065 ± 0.0003 b = 0.0052 ± 0.0007	0.79	0.63	202
HIX vs. $S_{250\text{-}600}$	Exponential y = a*exp(-b*x) + c	a = 0.175± 0.001 b = 1.032± 0.146 c = 0.025±0.001	0.83	0.69	202
HIX vs. S_R	Exponential y = a*exp(-b*x) + c	a = 1.530± 0.199 b = 1.242± 0.293 c = 2.602±0.066	0.64	0.41	202

All variables were fitted to the equation type in the second column. All regression coefficients and coefficients of determination are significant at a confidence level of $p<0.01$.

1064 Figure 1.
1065

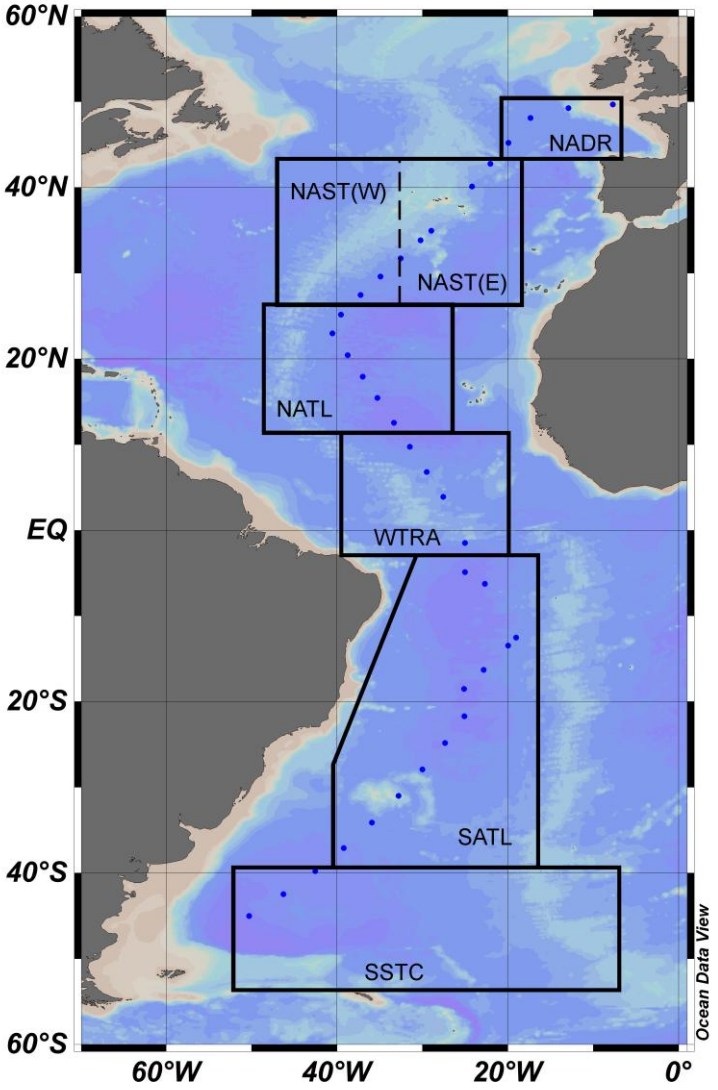

1066
1067 Figure 1. Location of sampling stations along the AMT 20 cruise track overlain on boundaries
1068 of bio-geographic provinces according to Longhurst (1995).
1069

Figure 2.

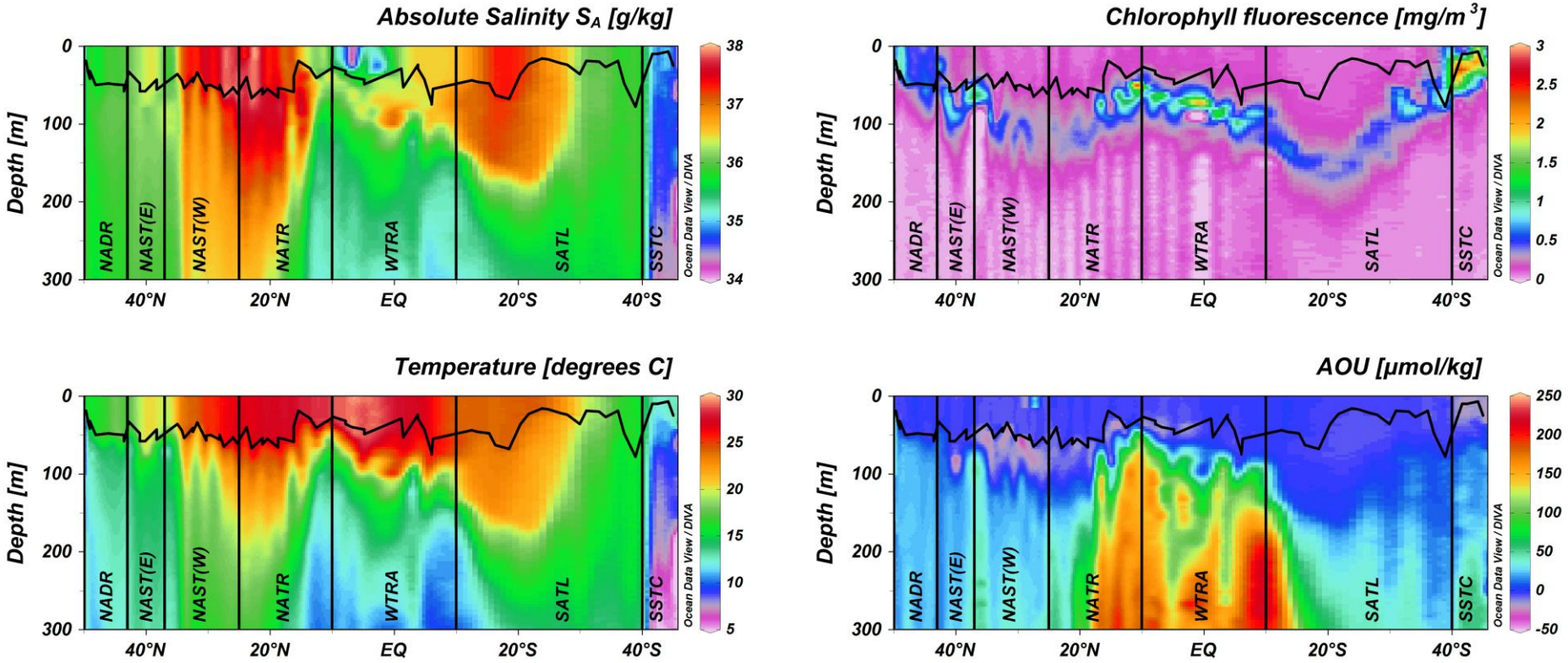

Figure 2. Meridional sections of Absolute Salinity (S_A), temperature, chlorophyll-*a* fluorescence and Apparent Oxygen Utilization. The solid line overlaid on the section plots represents the depth of the thermocline. The vertical line delineates boundaries of Longhurst (1995) biogeographic provinces.

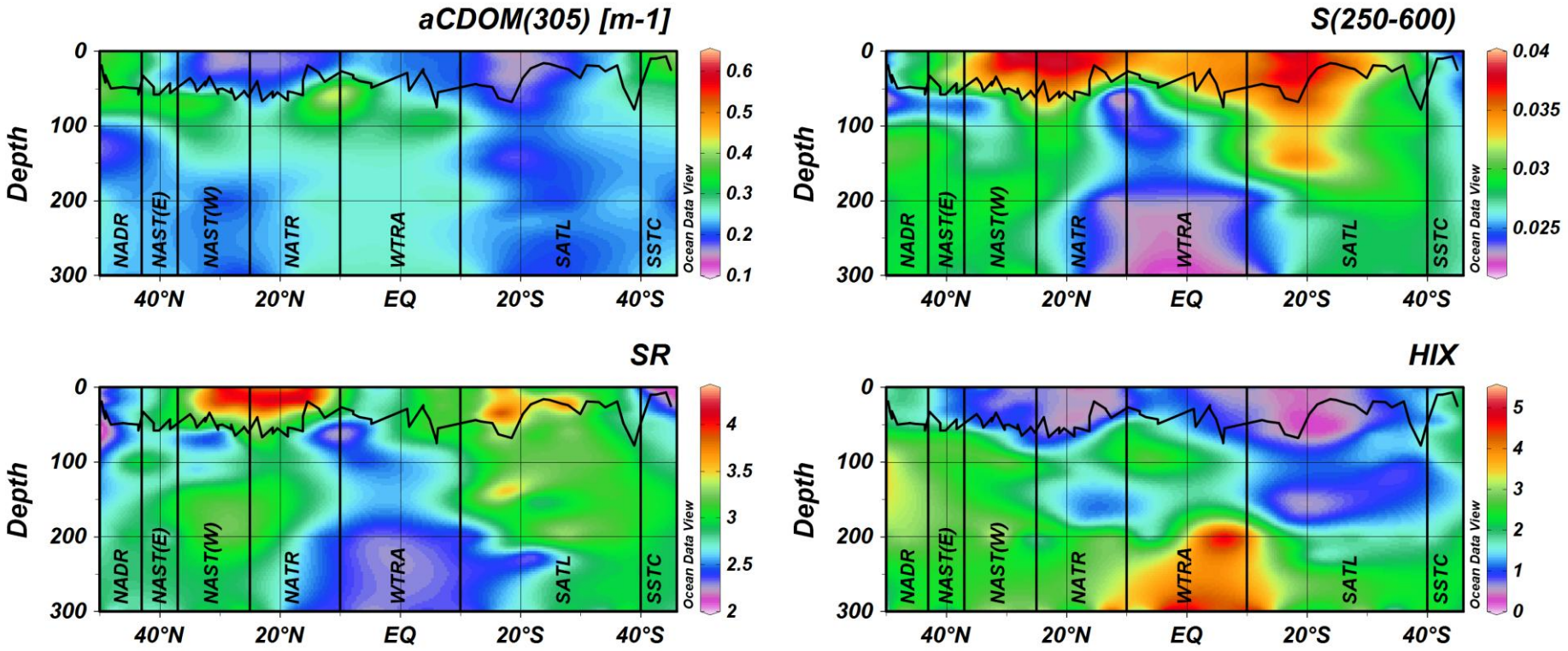

Figure 3. Meridional sections of the distribution of CDOM absorption coefficient, $a_{CDOM}(305)$, spectral slope coefficient, $S_{250\text{-}600}$, and spectral slope ratio, S_R and Humification Index – HIX. The solid line overlaid on the section plots represents the depth of the thermocline. The vertical line delineates boundaries of Longhurst (1995) biogeographic provinces.

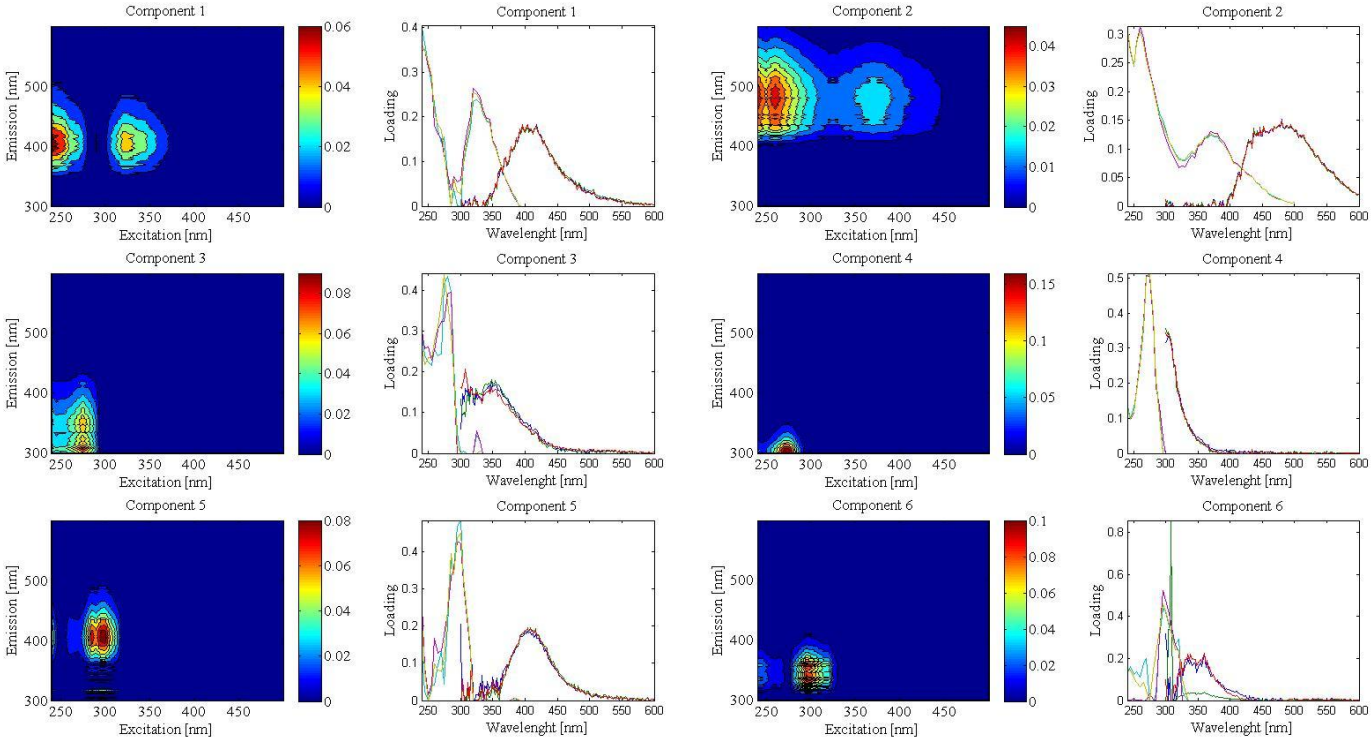

Figure 4. The PARAFAC model output showing fluorescence signatures of six components identified in the AMT20 data set. Contour plots present spectral shapes of excitation and emission of derived components. Components C1–C6 are ordered by decreasing percent of explained variation. Line plots at right side of each contour plot present split-half validation results for each identified component. Excitation (left) and emission (right) spectra were estimated from three independent 6-component PARAFAC models run on two random halves of the data set (CAL — blue lines, VAL — green lines) and the complete data set (red lines).

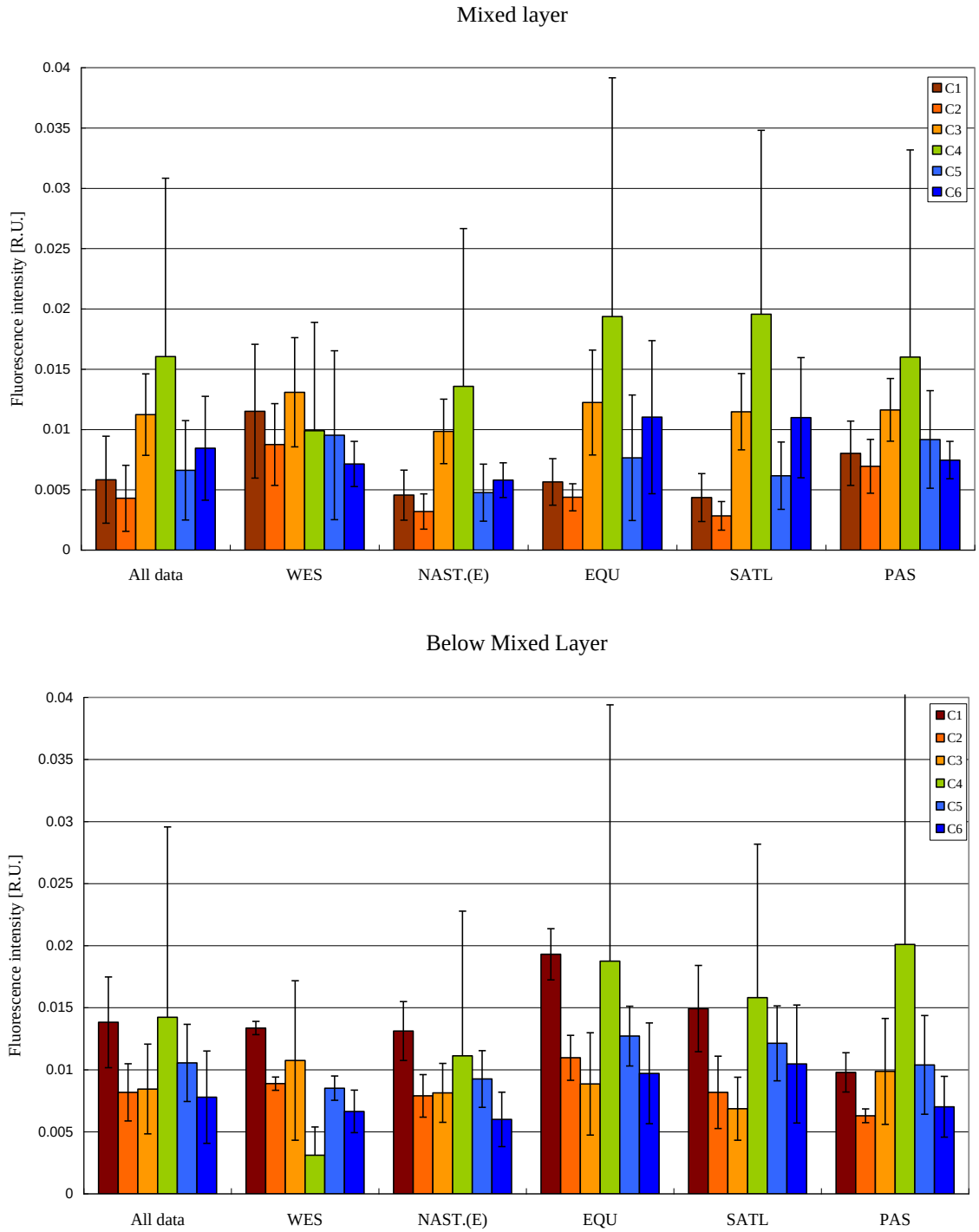

Figure 5. Composition of CDOM fluorescence excitation and emission matrix spectra in the mixed (upper graph) and below mixed layer (lower graph) in major biogeographic provinces of the Atlantic Ocean: WES - Western European Shelf, NAST(E) - North Atlantic Subtropical Gyre, EQU - Equatorial Upwelling, SATL - South Atlantic Subtropical Gyre, PAS - Patagonian Shelf. Bar plots represent average intensity of 6 components calculated for samples collected at a particular province and the depth range, the whisker represents the standard deviation.

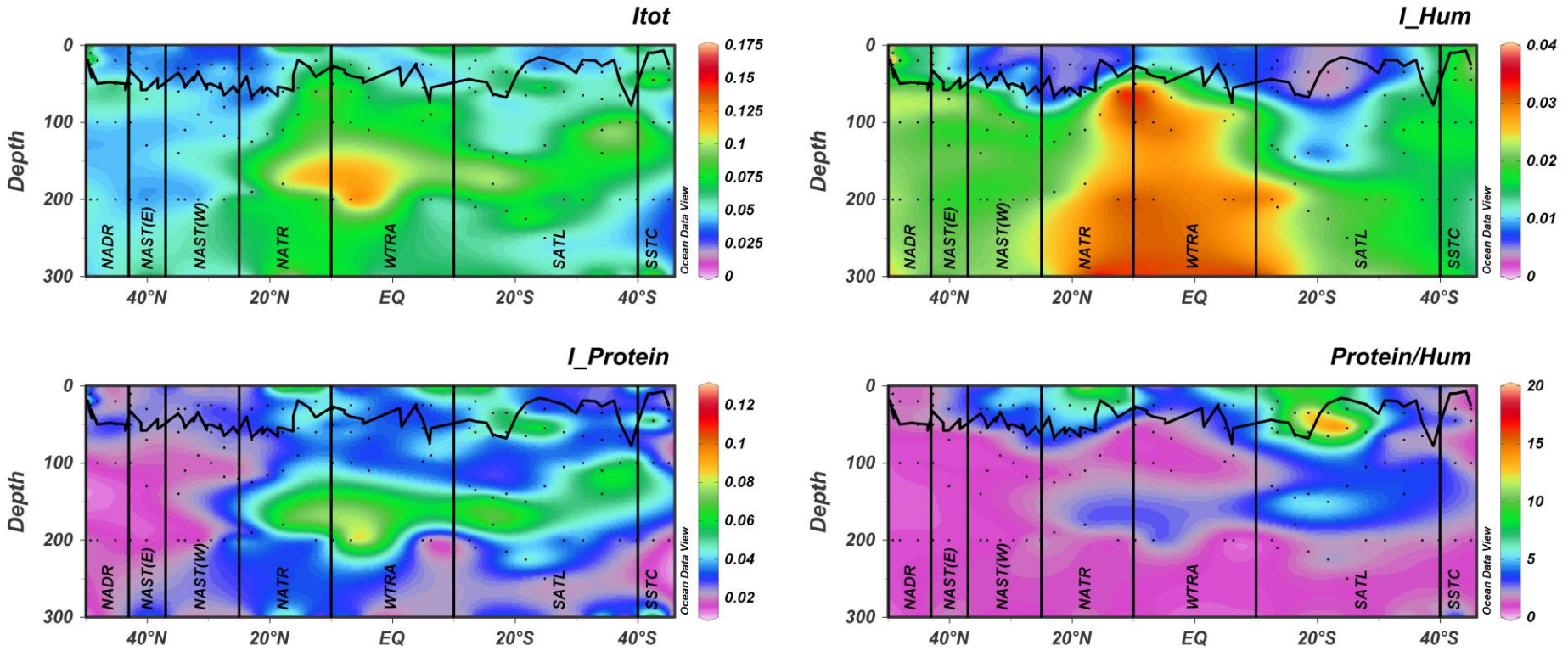

Figure 6. Meridional sections of the distribution of total DOM fluorescence intensity, I_{Tot}, intensity of the humic fraction of the DOM fluorescence, I_{Humic}, intensity of the protein-like fraction of the DOM fluorescence, $I_{Protein}$ and the ratio of respective DOM fluorescence fractions, $I_{Protein}/I_{Humic}$. The solid line overlaid on the section plots represents the depth of the thermocline. The vertical line delineates boundaries of Longhurst (1995) biogeographic provinces.

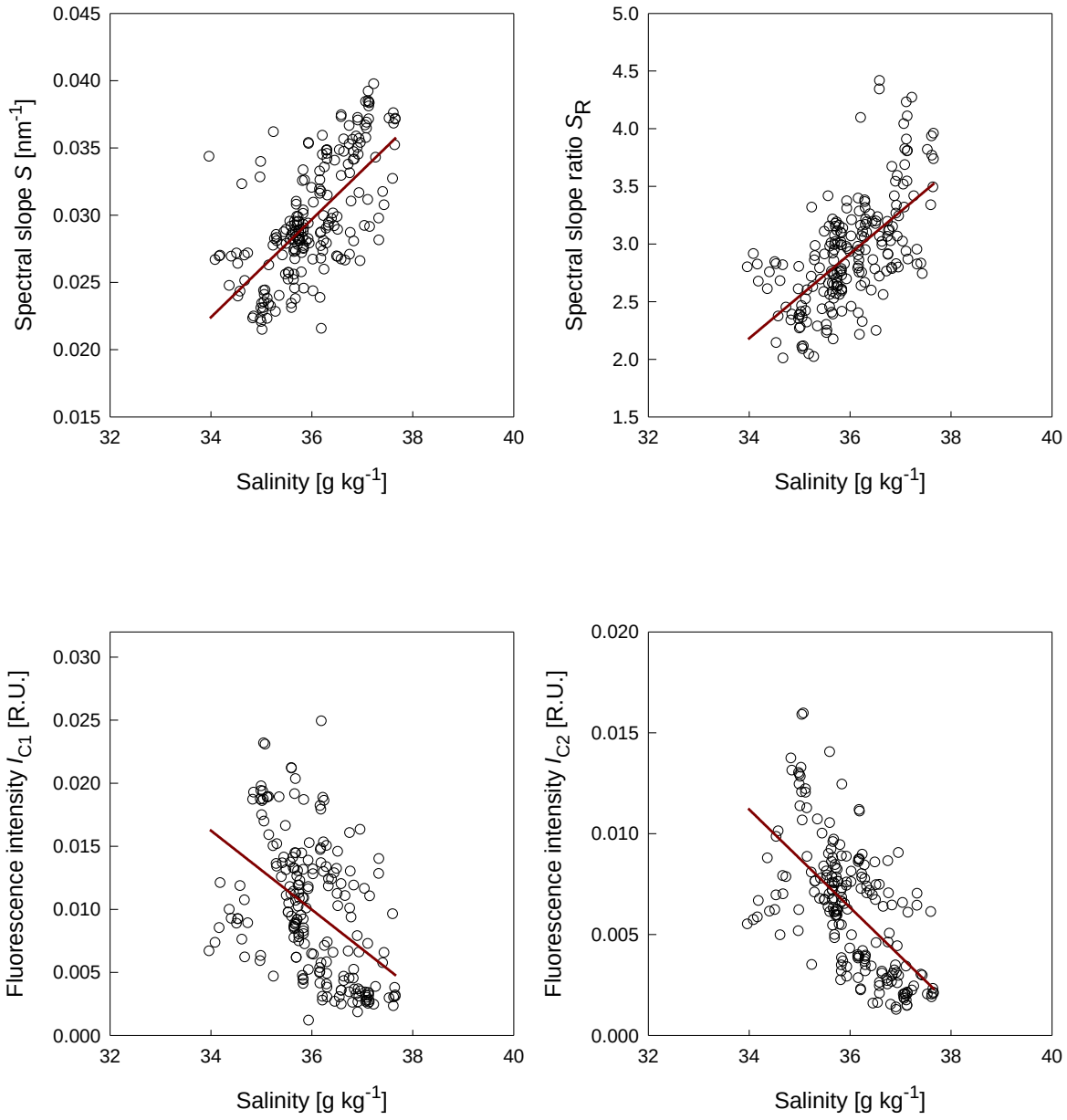

Figure 7. Relationships of the salinity and spectral slope coefficient, $S_{250\text{-}600}$, spectral slope ratio S_R, and fluorescence intensity of components C1 and C2, I_{C1}, I_{C2}, during the AMT20 cruise.

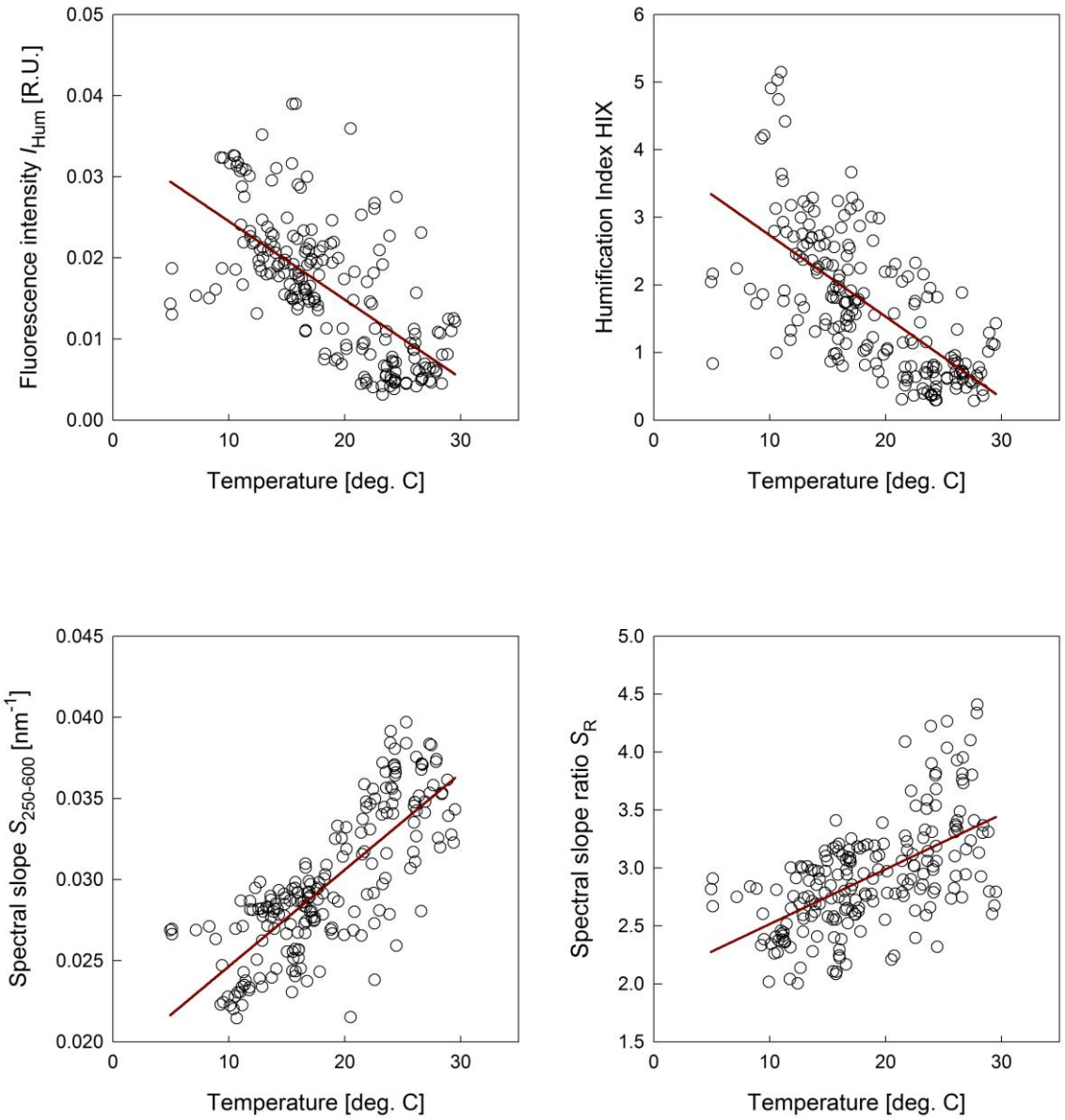

Figure 8. Distribution of the fluorescence intensity of humic like components I_{Humic}, humification index, HIX, spectral slope coefficient, $S_{250-600}$, and the spectral slope ratio S_R, in the function of water temperature during the AMT20 cruise.

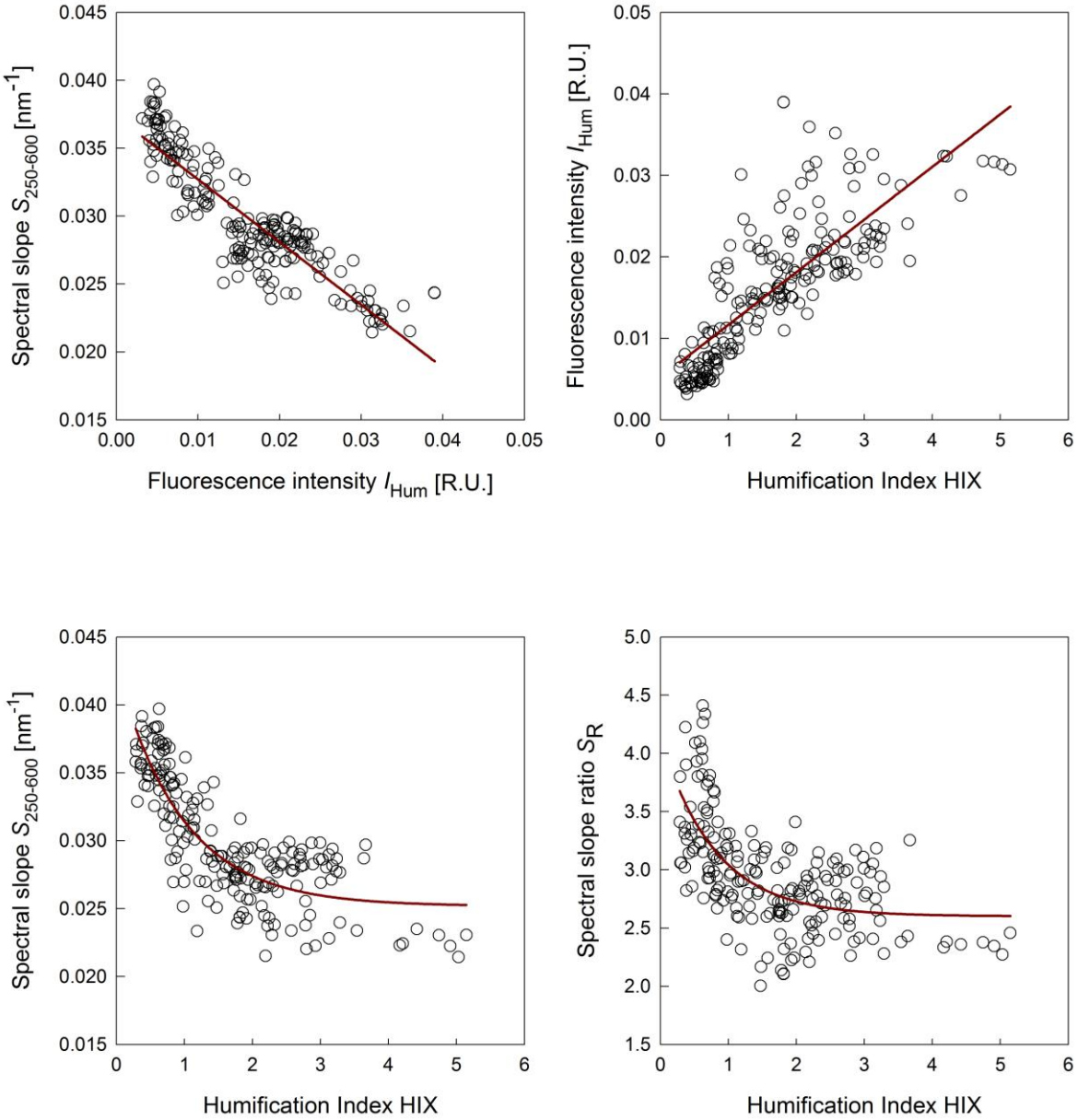

Figure 9. Relationships between fluorescence intensity of humic-like components, I_{Humic}, and spectral slope coefficient, $S_{250\text{-}600}$ (upper left panel). Relationships between Humification Index, HIX, and fluorescence intensity of humic-like components, I_{Humic}, spectral slope coefficient, $S_{250\text{-}600}$, and spectral slope ratio S_R (upper right and lower panels).

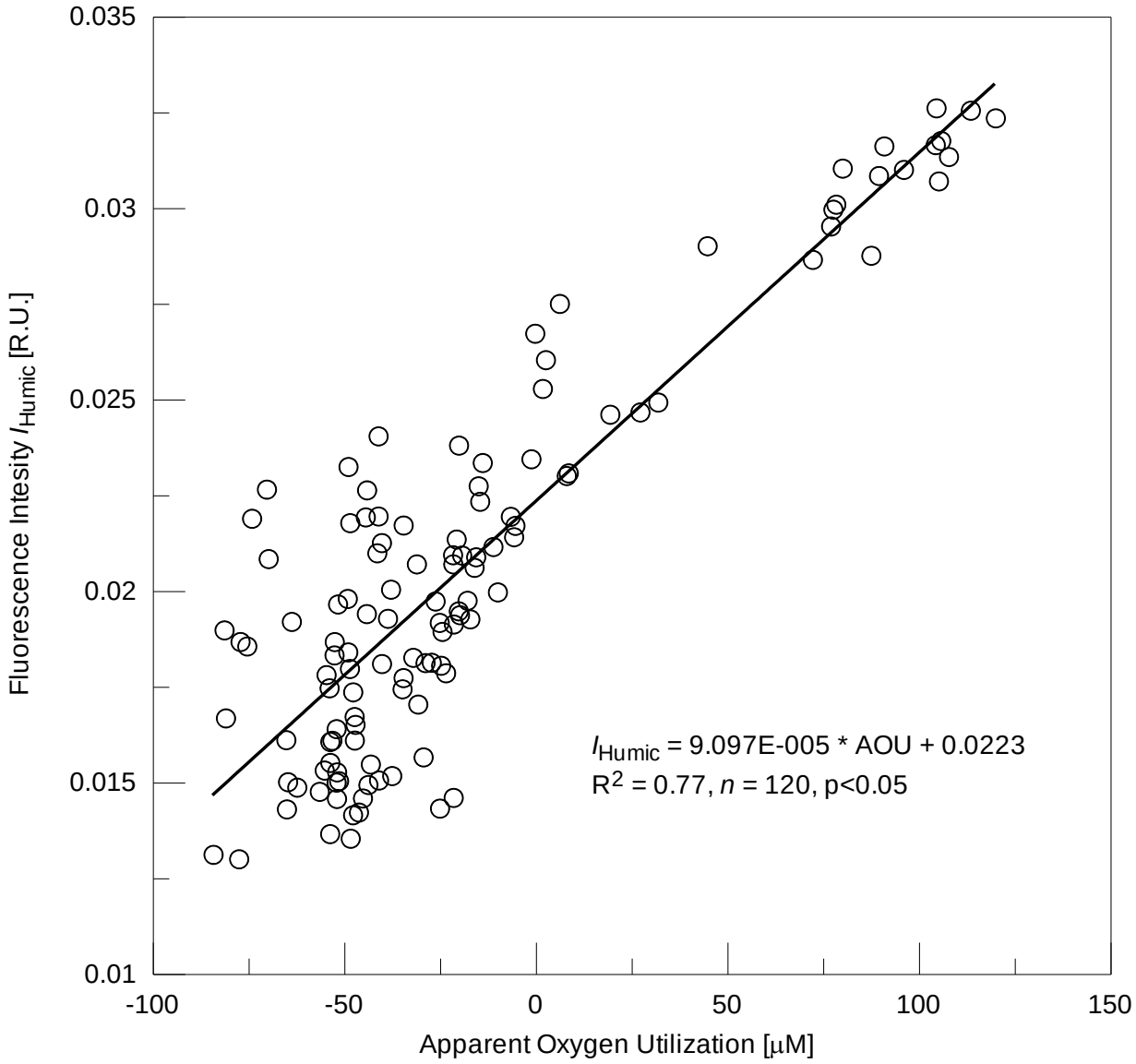

Figure 10. Relationship between Apparent Oxygen Utilization and the cumulative fluorescence intensity of humic-like components I_{Humic} in the Atlantic Ocean over the depth range of 140-300 m.